JOURNAL OF GEOPHYSICAL RESEARCH, VOL. 106, NO. D12, PAGES 12,381–12,400, JUNE 27, 2001

Numerical simulations of the July 10, 1996, Stratospheric-Tropospheric Experiment: Radiation, Aerosols, and Ozone (STERAO)-Deep Convection experiment storm: Redistribution of soluble tracers

M. C. Barth

National Center for Atmospheric Research, Boulder, Colorado

A. L. Stuart

Department of Civil and Environmental Engineering, Stanford University, Stanford, California

W. C. Skamarock

National Center for Atmospheric Research, Boulder, Colorado

Abstract. By using a three-dimensional convective cloud model to simulate the July 10, 1996, Stratospheric-Tropospheric Experiment: Radiation, Aerosols, and Ozone-Deep Convection experiment storm, we investigate the fate of tracers of varying solubilities in midlatitude convection. The tracer distribution resulting from the interactions of the soluble tracers with the cloud hydrometeors is illustrated for two cases. The first case assumes that the dissolved tracer in the cloud water or rain completely degasses when the parent hydrometeor is converted to ice, snow, or hail through microphysical processes. The second case assumes that the dissolved tracer is retained in the ice, snow, or hail. We find that when soluble tracers are degassed, both low- and high-solubility tracers are transported to the upper troposphere. When tracers are retained in ice hydrometeors, the highly soluble tracers are not ultimately transported to the upper troposphere but, instead, are precipitated out of the upper troposphere by snow and hail. Tracers of low solubility are transported upward, similar to passive tracer transport. The key microphysical processes that control these results are the accretion of cloud water by snow and hail. For the simulation in which retention of tracers in ice was considered, highly soluble scalars (10^5 M atm^{-1}) have a scavenging efficiency > 55% and have a mass change in the upper troposphere (8–15 km mean sea level) of -0.5 $\times$ 10^5 kg to 0 for a 3-hour period, while a passive scalar has a mass change of 2.3 $\times$ 10^5 kg.

1. Introduction

Deep convection has been known to be a primary mechanism of moving trace gas species from the boundary layer to the free troposphere [e.g., *Dickerson et al.*, 1987; *Chatfield and Crutzen*, 1984]. Chemical consequences of the transport of boundary layer air to the upper and middle troposphere on the regional scale can be to attain ozone (O_3) concentrations greater than if the atmosphere were undisturbed by convection [*Pickering et al.*, 1992b]. Recently, it has been hypothesized that deep convection can affect the odd hydrogen (HO_x) budget in the upper troposphere [*Prather and Jacob*, 1997; *Jaeglé et al.*, 1997]. However, studies have not examined in detail how deep convection processes the HO_x precursors, such as methyl hydrogen peroxide (CH_3OOH), hydrogen peroxide (H_2O_2), formaldehyde (CH_2O), and acetone. All of these species have some degree of solubility, so that they may be susceptible to scavenging, and some of these species undergo chemical reaction in the liquid drops.

To understand the influence of solubility, we use a three-dimensional cloud model to examine the evolution of tracers with different levels of solubility to determine to what degree soluble tracers are scavenged by a representation of the July 10, 1996, Stratospheric-Tropospheric Experiment: Radiation, Aerosols, and Ozone (STERAO)-Deep Convection experiment storm. Initially, each tracer has the same vertical mixing ratio profile, with high values in the boundary layer and lower values in the free troposphere. We also address the role that the frozen hydrometeors have on the soluble tracers through microphysical processes.

The goal of this paper is to learn what amount of soluble scalars are transported into the upper troposphere and what processes in the convection influence the distribution of the soluble scalars. Past studies have examined the flux of pas-

Paper number 2001JD900139.
0148-0227/01/2001JD900139$09.00

sive insoluble tracers, such as carbon monoxide (CO) and ozone (O_3), by deep convection from the boundary layer to the upper troposphere [e.g., *Pickering et al.*, 1992a]. The results of these studies have indicated that transport of boundary layer air to the anvil depends strongly on storm dynamics and, in particular, the degree of entrainment that occurs in any one storm. For example, *Scala et al.* [1990] found that because of the presence of a midlevel inflow jet and a strong melting layer in a tropical convective storm observed in Brazil, the vertical development of a core updraft was reduced. They found that > 50% of the air in the anvil originated from above 6 km in altitude. On the other hand, *Hauf et al.* [1995] found boundary layer air that had not been diluted up to 120 km downwind of the updraft core in a thunderstorm observed in southern Germany. *Pickering et al.* [1992b] and *Scala et al.* [1993] simulated three central United States squall lines to examine tracer transport. For these simulated storms, *Thompson et al.* [1994] reported net transport rates of 7–12% of a boundary layer tracer to the free troposphere over a horizontal domain of 240–320 km. From these results, *Thompson et al.* [1994] estimated the net flux of CO from the boundary layer (1.5 km prescribed depth) to the free troposphere due to deep convection to be 1–10 × 10^7 kg CO per month for northeast Colorado (40-42.5°N, 102.5-105°W).

Some studies have examined the budgets of reactive soluble species in convection. *Tremblay* [1987] calculated vertical transport rates, defined as the ratio of the cumulative mass transported across a level in the upper portion of a cloud to the amount of the species initially below that level in the 12 x 12 km model domain. The vertical transport rate was < 0.4% per hour through small convective storms for sulfur dioxide, which was subject to both scavenging and in-cloud oxidation. *Wang and Crutzen* [1995] found, from their two-dimensional (2-D) simulation of a midlatitude cumulonimbus, that dilution of boundary layer air with free troposphere air was considerable. Coupling this detrainment with SO_2 scavenging and aqueous oxidation resulted in SO_2 in the anvil region being < 10% of the initial boundary layer SO_2. *Flossmann and Wobrock* [1996] simulated medium-sized convection observed during the Global Atmospheric Research Program (GARP) Atlantic Tropical Experiment (GATE) and also found very little venting of sulfur dioxide from the boundary layer to the free troposphere, again because of in-cloud oxidation.

Very little work has been performed which systematically assesses the importance of scavenging on the redistribution of chemical species. The studies mentioned above either have not quantitatively assessed the redistribution of soluble chemical species or have initialized the concentrations of different chemical species with distinct vertical profiles. Furthermore, many studies have focused on species, such as sulfur dioxide and hydrogen peroxide, that undergo both scavenging into the liquid hydrometeors and aqueous reaction. *Crutzen and Lawrence* [2000] used a global chemistry transport model to study the effect of precipitation scavenging on the transport of trace gases. By initializing the trace gases to the same values and assigning different solubilities to each trace gas, *Crutzen and Lawrence* [2000] found that the mixing ratio of trace gases with a Henry's law coefficient of 10^3, 10^4, and 10^5 M atm^{-1} are reduced in the middle to upper troposphere by 20%, 60%, and 90%, respectively.

The study presented here quantitatively examines the redistribution of nonreactive, soluble species by deep convection. It is important to study systematically the effects of scavenging in an isolated manner so that coupled effects of scavenging, chemistry, and transport can be better understood in comprehensive models. This study is performed with three-dimensional simulations rather than two-dimensional simulations that are then extrapolated in the third dimension. This is particularly important in that most convection is of a three-dimensional nature [*Skamarock et al.*, 2000], as is the storm simulated in this study.

A detailed description of how a soluble trace gas is scavenged by the liquid hydrometeors follows. In this description we explain the importance of the microphysical processes and outline the methodology used to determine the dissolved tracers' fate when the liquid hydrometeor is converted to the frozen phase. Results of the simulations are presented with a subsequent discussion.

2. Model Description

2.1. Model Initialization

The cloud model used for the simulations is the three-dimensional, fully compressible, nonhydrostatic Collaborative Model for Multiscale Atmospheric Simulation (COMMAS), which is derived from the *Wicker and Wilhelmson* [1995] model. This model uses a Van-Leer type, monotonic

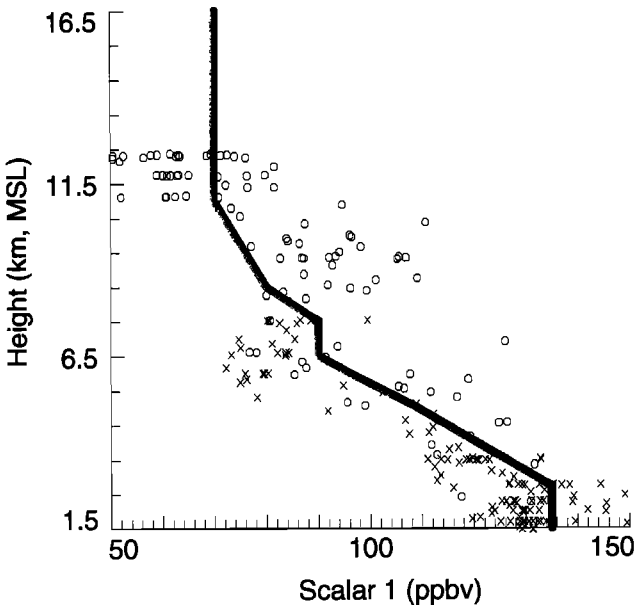

Figure 1. Initial concentration of the passive and soluble tracers used in the simulation. This profile represents the CO aircraft measurements (points) obtained outside of the storm during the July 10, 1996, Stratospheric-Tropospheric Experiment: Radiation, Aerosols, and Ozone (STERAO) storm. Adapted from *Skamarock et al.* [2000].

Table 1. Solubilities and Accommodation Coefficients of Soluble Tracers

Scalar	Solubility, M atm^{-1}	Accommodation Coefficient
1	0.	$5. \times 10^{-3}$
2	0.	5.3×10^{-4}
3	$1. \times 10^{-3}$	$5. \times 10^{-3}$
4	$1. \times 10^{-2}$	5.3×10^{-4}
5	$1. \times 10^{-1}$	$5. \times 10^{-3}$
6	$1. \times 10^{0}$	$5. \times 10^{-3}$
7	$5. \times 10^{0}$	$5. \times 10^{-2}$
8	$1. \times 10^{1}$	$5. \times 10^{-2}$
9	$5. \times 10^{1}$	$5. \times 10^{-2}$
10	$1. \times 10^{2}$	$5. \times 10^{-2}$
11	$5. \times 10^{2}$	$5. \times 10^{-2}$
12	$1. \times 10^{3}$	$2. \times 10^{-1}$
13	$5. \times 10^{3}$	$2. \times 10^{-2}$
14	$1. \times 10^{4}$	$2. \times 10^{-1}$
15	$1. \times 10^{5}$	$2. \times 10^{-1}$
16	$1. \times 10^{6}$	$2. \times 10^{-1}$
17	$1. \times 10^{7}$	$2. \times 10^{-1}$
18	$1. \times 10^{12}$	$1. \times 10^{-1}$

advective scheme [*Wicker and Wilhelmson*, 1995] to transport water vapor q_v, cloud water q_c, rain q_r, cloud ice q_i, snow q_s, graupel or hail q_g, and scalars. A second-order Runge-Kutta time integration [*Wicker and Skamarock*, 1998] is used to advance the quantities in time. The ice microphysics parameterization is that described by *Tao and Simpson* [1993], which is based on *Lin et al.* [1983]. For the simulations performed here, hail hydrometeor characteristics (ρ_h = 0.9 g cm^{-3}, $N_o = 4 \times 10^4$ m^{-4}) are used.

The model is configured to a 120 x 120 x 20 km domain with 121 grid points in each horizontal direction (1-km resolution) and 51 grid points in the vertical direction with a variable resolution beginning at 50 m at the surface and stretching to 700 m at the top of the domain. A description of the meteorological scenario and transport of passive tracers is given by *Skamarock et al.* [2000] for the July 10, 1996, STERAO storm. We initialize the model environment and the initiation of convection in the same manner as *Skamarock et al.* [2000].

Skamarock et al. [2000] initialized two passive tracers, representative of CO and O_3, using measurements obtained by the aircraft outside of cloud. The passive tracer representing CO is included in the simulations performed for this study, and its initial profile is shown in Figure 1. This study includes an additional 16 tracers of variable solubility (Table 1), whose initial profiles are the same as the CO initial profile. Thus we can directly compare the effect of solubility on the redistribution of a tracer by convection.

The initial profile used here does not necessarily represent vertical profiles of all soluble species, although there are similar characteristics between the initial profiles of soluble species and CO. For northeastern Colorado, which can be influenced by the Denver metropolitan area and other Front Range communities, several soluble species, e.g., CH_2O, HNO_3, and SO_2, have a boundary layer source similar to the one shown in Figure 1. However, in the free troposphere these species decrease to concentrations that are < 10% of their boundary layer concentration (except for HNO_3, which decreased to half its boundary layer concentration). The peroxides generally have a peak concentration at 4 km mean sea level (MSL) and decrease in the free troposphere to small cocentrations (<10% of peak value). The sensitivity of our results to the initial profile is discussed in section 3.3.

2.2. Sources and Sinks of the Soluble Tracers

The conservation equation for a soluble scalar can be expressed as

$$\frac{\partial(\bar{\rho}C_{\text{gas}})}{\partial t} = -\frac{\partial(\bar{\rho}uC_{\text{gas}})}{\partial x} - \frac{\partial(\bar{\rho}vC_{\text{gas}})}{\partial y} - \frac{\partial(\bar{\rho}wC_{\text{gas}})}{\partial z} + \left.\frac{\partial(\bar{\rho}C_{\text{gas}})}{\partial t}\right|_{\text{MT}}, \quad (1)$$

$$\frac{\partial(\bar{\rho}C_{\text{liq}})}{\partial t} = -\frac{\partial(\bar{\rho}uC_{\text{liq}})}{\partial x} - \frac{\partial(\bar{\rho}vC_{\text{liq}})}{\partial y} - \frac{\partial(\bar{\rho}wC_{\text{liq}})}{\partial z} + \left.\frac{\partial(\bar{\rho}C_{\text{liq}})}{\partial t}\right|_{\text{MT}} + \left.\frac{\partial(\bar{\rho}C_{\text{liq}})}{\partial t}\right|_{\text{MP}} + \left.\frac{\partial(\bar{\rho}fC_{\text{liq}})}{\partial t}\right|_{\text{Sed}}, \quad (2)$$

where C_{gas} and C_{liq} are the mixing ratio of a soluble scalar in the gas phase and liquid phase. Here, $\partial(\bar{\rho}C_{\text{gas}})/\partial t|_{\text{MT}}$ and $\partial(\bar{\rho}C_{\text{liq}}/\partial t)|_{\text{MT}}$ account for the mass transfer (MT) of a scalar between the gas and liquid phases. Adsorption of gas-phase species onto ice, snow, or hail is not considered in this study. The $\partial(\bar{\rho}C_{\text{liq}})/\partial t|_{\text{MP}}$ accounts for the transfer of the dissolved scalar among hydrometeors through microphysics; $\partial(\bar{\rho}fC_{\text{liq}})/\partial t|_{\text{Sed}}$ accounts for the sedimentation of a chemical species in rain, where f represents the fraction of the liquid that is in rain. The first three terms on the right-hand side of (1) and (2) describe the advection of the scalar species. The calculation of C_{gas} and C_{liq} at time step $t + \Delta t$ is performed via time splitting. Intermediate values of C_{gas} and C_{liq} are determined first from calculating the advection of the scalar species. These intermediate values are then used for the calculation of the transfer by microphysical processes ($\partial(\bar{\rho}C_{\text{liq}})/\partial t|_{\text{MP}}$) and sedimentation of species in rain ($\partial(\bar{\rho}fC_{\text{liq}})/\partial t|_{\text{Sed}}$) to attain second intermediate values. These new values are used for the calculation of the dissolution and volatization of the scalar between the gas and liquid phases to attain the final values of C_{gas} and C_{liq} for the time step. The details of $\partial(\bar{\rho}C_{\text{gas}})/\partial t|_{\text{MT}}$, $\partial(\bar{\rho}C_{\text{liq}})/\partial t|_{\text{MT}}$, $\partial(\bar{\rho}C_{\text{liq}})/\partial t|_{\text{MP}}$, and $\partial(\bar{\rho}fC_{\text{liq}})/\partial t|_{\text{Sed}}$ are now described.

2.2.1. Mass transfer between gas and aqueous phases. The absorption of a chemical species in the gas phase into the cloud water and rain is determined by either Henry's law equilibrium or by mass transfer limitation calculations. Henry's law equilibrium can relate the aqueous phase concentration of a chemical species [X] to the gas-phase concentration of the chemical species (p_X),

$$[\mathrm{X}] = K_H\, p_X, \tag{3}$$

where [X] is in units of mol X/L H_2O or M, K_H is the Henry's law coefficient (M atm^{-1}), and p_X is in units of atm X. The phase ratio P_x is defined as the ratio of the concentration of a chemical species in the aqueous phase (C_{liq}, molecule cm^{-3}) to that in the gas phase (C_{gas}, molecule cm^{-3}) [*Lelieveld and Crutzen*, 1991] and for a species in Henry's law equilibrium can be determined as,

$$P_x = K_H\, R\, T\, L_{\mathrm{tot}}, \tag{4}$$

where R (L atm mol^{-1} K^{-1}) is the universal gas constant, T (K) is temperature, and L_{tot} (cm^3 H_2O cm^{-3} air) is the liquid water content including both cloud water and rain. A relationship between the chemical concentration in the liquid phase and the total concentration (C_{tot}, molecule cm^{-3}) is found using the phase ratio,

$$C_{\mathrm{liq}} = \frac{P_x}{1 + P_x}\, C_{\mathrm{tot}}. \tag{5}$$

However, a chemical species may not attain equilibrium on the timescales of the cloud model's timestep because of slow mass transfer between phases [*Schwartz*, 1986]. The rate of change of a chemical species due to mass transfer between gas and liquid phases is

$$\left.\frac{\partial(\bar{\rho} C_{\mathrm{liq}})}{\partial t}\right|_{\mathrm{MT}} = \bar{\rho}\, k_t\, L_{\mathrm{tot}}\, C_{\mathrm{gas}} - \frac{\bar{\rho}\, k_t}{K_H\, R\, T}\, C_{\mathrm{liq}}. \tag{6}$$

Specifically for cloud water and rain,

$$\left.\frac{\partial(\bar{\rho} C_{cw})}{\partial t}\right|_{\mathrm{MT}} = \bar{\rho}\, k_{tc}\, L_c\, C_{\mathrm{gas}} - \frac{\bar{\rho}\, k_{tc}}{K_H\, R\, T}\, C_{cw}, \tag{7}$$

$$\left.\frac{\partial(\bar{\rho} C_r)}{\partial t}\right|_{\mathrm{MT}} = \bar{\rho}\, k_{tr}\, L_r\, C_{\mathrm{gas}} - \frac{\bar{\rho}\, k_{tr}}{K_H\, R\, T}\, C_r, \tag{8}$$

where the additional c or r subscript denotes that parameter for the cloud water or rain characteristics. For the gas-phase species,

$$\left.\frac{\partial(\bar{\rho} C_{\mathrm{gas}})}{dt}\right|_{\mathrm{MT}} = \bar{\rho}\frac{k_{tc} C_{cw} + k_{tr} C_r}{K_H\, R\, T} - \bar{\rho}(k_{tc}\, L_c + k_{tr}\, L_r)\, C_{\mathrm{gas}}, \tag{9}$$

where

$$k_t = (\tau_{Dg} + \tau_i)^{-1}. \tag{10}$$

In this study, it is assumed that diffusion through the gas phase and across the interface of the liquid drop can be represented by the first-order rate constant k_t [cm^3 air (cm^3 H_2O)$^{-1}$ s^{-1}] and that diffusion inside the cloud or rain drops is not rate limiting (that is, the drops are well mixed) and thus is neglected. Here τ_{Dg} is the gas diffusion timescale and τ_i is the timescale for transfer across the interface of the liquid drop.

$$\tau_{Dg} = \frac{\bar{a}^2}{3 D_g}. \tag{11}$$

$$\tau_i = \frac{4\bar{a}}{3\nu\alpha}. \tag{12}$$

Here $\bar{a}$ is the mass mean radius (10 μm for cloud drops, 2 λ^{-1} for rain drops, where λ is the slope in the raindrop size distribution), D_g is the diffusivity of the species in the gas phase (0.1 cm^2 s^{-1} is used in this study), ν is the thermal velocity of the species, and α is the species-dependent accommodation coefficient (Table 1). The accommodation coefficient values are assigned according to the solubility of the scalar. For example, soluble species such as HO_2, CH_2O, H_2O_2, and HNO_3 have solubilities of 10^3 M atm^{-1} and greater, and these species have higher accommodation coefficients [*Lelieveld and Crutzen*, 1991].

We calculate the amount of a chemical species that would transfer from the gas phase to the cloud and rain hydrometeors according to (6)-(9) during a single time step. We also calculate the amount of a chemical species that would reside in the liquid hydrometeors (cloud plus rain) under Henry's law equilibrium (equation (5)). If the amount under Henry's law equilibrium is less than the amount transferred by the mass transfer equations, then we simply partition the chemical species between the gas phase and liquid hydrometeors following Henry's law equilibrium. This generally occurs with scalars 3–10 (see Table 1) for the 6-s time step. Further partitioning is needed between the cloud water and rain, and this is accomplished by using the fraction of the sum of the cloud water and rain mixing ratios that occurs as cloud water. If Henry's law equilibrium cannot be applied, then (7)-(9) are used to determine the amounts of the chemical species in the gas phase, cloud water, and rain.

2.2.2. Mass transfer between cloud hydrometeors. Once a soluble tracer is dissolved into the cloud water and rain drops, it is subject to transfer through the microphysical processes that affect the parent hydrometeor. A similar approach was followed by *Rutledge et al.* [1986].

The effects of microphysical processes that transfer water from liquid-phase hydrometeors to solid- or mixed-phase hydrometeors on chemical distributions are poorly understood. During formation and growth of solid- or mixed-phase hydrometeors via freezing, riming, or depositional growth at the expense of liquid water, trace chemical species originally in the aqueous phase may be excluded or captured by the growing ice phase. During freezing and riming, expulsion of solutes may occur through exclusionary crystal growth or diffusion of solutes in the liquid phase with subsequent volatilization at the liquid-gas interface. Mechanisms of retention in the solid- or mixed-phase hydrome-

teor include incorporation of solute ions in the solid crystal structure, trapping of solutes in spaces in the crystal structure or interstitial spaces between crystals, and dissolution in remaining liquid phase. Trace species may also be incorporated in ice growing via deposition, by adsorption at the solid surface or in a quasi-liquid surface layer, and by incorporation in the bulk ice phase via diffusion or due to repavement of the surface by depositing water molecules. (See *Hobbs* [1974] and *Pruppacher and Klett* [1997] for a detailed discussion of these processes.)

In cold clouds the collision of supercooled droplets with solid ice and their subsequent freezing (called riming) is known to lead to the efficient retention of nonvolatile species such as sulfate [e.g., *Borys et al.*, 1983; *Mitchell and Lamb*, 1989]. The degree of retention of more volatile species during hydrometeor freezing is much less well characterized. Several laboratory and field observational studies have measured retention efficiencies of gases in freezing substrates for a limited number of chemical species found in clouds, including H_2O_2, SO_2, O_2, HCl, NH_3, and HNO_3 [*Lamb and Blumenstein*, 1987; *Iribarne and Pyshnov*, 1990; *Snider et al.*, 1992; *Snider and Huang*, 1998]. The retention efficiency represents the concentration of solute in the solid phase versus that in the original liquid hydrometeor. These studies have resulted in varying estimates of retention efficiencies (sometimes for the same gas), ranging from 0.01 to 1, without clear theoretical justification for the variation.

Adsorptive capture of chemical species by ice particles has been studied by many researchers in both the stratospheric and tropospheric chemistry fields [e.g., *Tabazadeh and Turco*, 1993; *Clapsaddle and Lamb*, 1989]. Experimental studies considering uptake found that the degree of uptake depends on many factors, including whether the ice phase is growing or not [*Diehl et al.*, 1995]. Although a few tropospheric cloud modeling studies have begun to parameterize and incorporate this process [e.g., *Rutledge et al.*, 1986; *Chen and Lamb*, 1990], we focus primarily on the effects of solute retention during freezing in this work and use a parameterization that only includes some adsorptive uptake during deposition growth at the expense of cloud water (i.e., the Bergeron process). In their Lagrangian air parcel cloud modeling study, *Chen and Lamb* [1990] noted that retention of SO_2 by riming was a much greater contributor to precipitative removal of trace species than capture by gas sorption (under both depositional growth and nongrowth conditions). Furthermore, the importance of solute retention at different levels in the cloud depended on the pathway of frozen hydrometeor growth (riming or deposition). Results from our cloud model simulation indicate that riming dominates in the updraft cores from 5-9 km MSL, while vapor deposition onto ice dominates above 9 km MSL. Vapor deposition onto precipitation (snow or hail) is small, thus redistribution of soluble tracers by direct adsorption may be small for this case.

In recent years, cloud chemistry modeling studies have begun to include the freezing transport mechanism for a limited number of volatile chemical species using representative retention efficiencies [*Wang and Chang*, 1993a; *Chen and Lamb*, 1994; *Kreidenweis et al.*, 1997; *Rutledge et al.*, 1986]. Modeling studies that have examined the effects of this mechanism have found that including solutes in the solid phase impacts chemical distributions and their time evolution [*Chen and Lamb*, 1990; *Wang and Chang*, 1993b], and can increase chemical deposition from precipitation [*Cho et al.*, 1989]. Since much remains unknown about how this process affects chemical distributions and previous work indicates potentially significant impacts, a better understanding of the effects of retention in the ice phase on soluble tracer transport is necessary.

In this study we perform two distinct modeling simulations. The first assumes all the soluble scalar is transferred from the liquid phase to the gas phase when a hydrometeor undergoes a conversion from liquid to solid (via freezing and evaporation/deposition processes). The second assumes all the soluble scalar is transferred to the resultant ice-containing hydrometeor. Because experimental results of the retention efficiency of solutes during freezing of liquid drops vary between 0.1 and 1, these two simulations provide bounding estimates of the actual retention of soluble tracers. Note that these bounding estimates are applicable to only the retention of soluble tracers during the conversion of liquid drops to frozen hydrometeors and do not include bounding estimates of direct adsorption of gases onto ice nor additional entrainment of the gas-phase scalar during the deposition stage of the Bergeron process. Thus we use a reasonable representation of the upper bound on retention and capture during liquid to solid hydrometeor transformation in order to examine the likely effects on soluble tracer fate. The actual upper bound could possibly reside outside this range owing to additional adsorption. Until adsorption processes are better understood and well represented in the cloud chemistry model, the effects of adsorption for this case cannot be quantified.

In general, the transfer of a soluble tracer from one hydrometeor to another is determined to be proportional by mass to the transfer of water from one hydrometeor to another,

$$\left.\frac{\partial(\bar{\rho}C_{\mathrm{X}})}{\partial t}\right|_{\mathrm{MP}} = MP_{\mathrm{X}}\,\frac{\bar{\rho}C_{\mathrm{Y}}}{q_{\mathrm{Y}}}, \tag{13}$$

where subscripts X and Y refer to the two hydrometeor categories, and MP_{X} is the source rate of the water from hydrometeor Y to hydrometeor X. Sedimentation of a soluble species in a precipitating hydrometeor is calculated as its mass flux through the model layer.

$$\left.\frac{\partial(\bar{\rho}C_{\mathrm{X}})}{\partial t}\right|_{\mathrm{Sed}} = \frac{\partial(\bar{\rho}V_{\mathrm{X}}C_{\mathrm{X}})}{\partial z}, \tag{14}$$

where subscript X refers to the precipitating hydrometeor class and V_{X} is the fall speed of the hydrometeor.

For the simulation where the soluble tracer degasses when liquid drops are converted to the frozen hydrometeor, the soluble tracer is transferred from the cloud water to rain when microphysical processes transfer cloud water to rain. For all microphysical processes that transfer the cloud water or rain to ice, snow, or hail, the dissolved scalar is transferred to the

gas phase. Rain-out of the scalar is determined similarly to (14).

For the second simulation, which assumes that the soluble scalars are retained during the conversion of liquid drops to the frozen hydrometeors, the dissolved scalar is transferred from the cloud water to rain when the microphysical processes transfer the cloud water to rain. For all microphysical processes that transfer the cloud water or rain to ice, snow, or hail, the dissolved scalar is transferred to the resultant frozen hydrometeor proportionally by mass. Likewise, microphysical processes that transfer ice to snow or hail or transfer snow to hail also transfer the dissolved scalar. Melting of ice, snow, or hail transfers the dissolved scalar to the cloud water or rain. During sublimation of the snow or hail, dissolved tracers are retained in the snow or hail unless all the hydrometeor mass is converted to the gas phase. Sedimentation of the scalar in the rain, snow, or hail is determined by its mass flux through the model layer (equation (14)).

3. Results

Observations of the July 10, 1996, STERAO storm showed that the storm evolved from a multicellular convective system to a supercellular system. These observations [*Dye et al.*, 2000] included satellite, radar, interferometer lightning data, and in situ chemistry and physics aircraft data of the inflow and anvil regions. Soluble tracers (e.g., HNO_3, H_2O_2, CH_2O, and SO_2) were measured in only the inflow region of this particular storm, and insoluble tracers (e.g., O_3, NO, and CO) were measured in both the inflow and outflow regions. Thus for this storm we cannot compare our soluble tracer model results to observations. Some soluble tracers were measured in the outflow of the July 12, 1996, STERAO storm, and analysis of these measurements will occur in a future study.

The results of the storm structure and dynamics presented here are representative of the storm that was observed (as is described by *Skamarock et al.* [2000]). Thus the evolution of the soluble tracers in this simulation of the July 10 STERAO convective system is likely representative of multicells and quasi-supercells, which are often observed in continental midlatitudes. However, it is difficult to generalize these results to other types of convection. Only after examining with observations and modeling studies the redistribution of soluble tracers in marine, tropical, and other continental convection can we begin to generalize our findings.

3.1. Hydrometeor Results

The storm structure, physics, and dynamics are described by *Skamarock et al.* [2000]. The simulated radar reflectivity from the 3-hour integration showed that the simulated storm

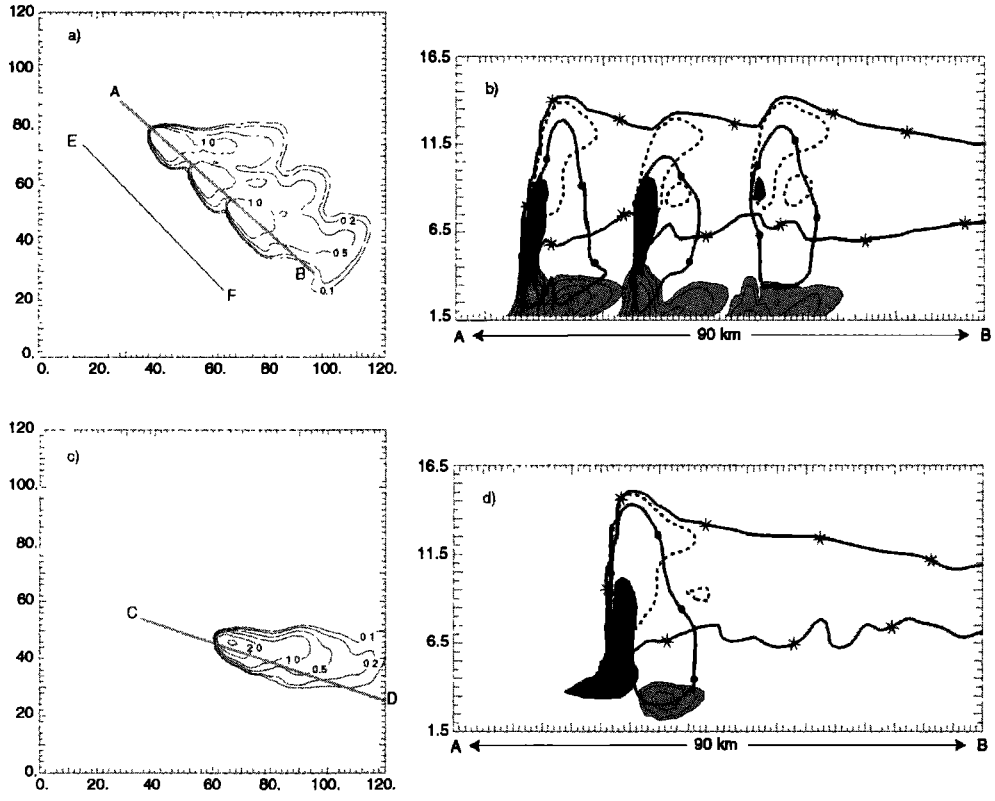

Figure 2. Hydrometeor mixing ratios (g kg^{-1}) for (a) snow at 11.5 km mean sea level (MSL) and t = 3600 s; (b) cloud water (dark-shaded region), rain (light-shaded region), ice (dotted line), snow (solid line with stars), and hail (solid line with solid circles) along the AB cross section at t = 3600 s; (c) snow at 11.5 km MSL and t = 9000 s; and (d) cloud water (dark-shaded region), rain (light-shaded region), ice (dotted line), snow (solid line with stars), and hail (solid line with solid circles) along the CD cross section at t = 9000 s. Contour levels for cloud water and rain mixing ratios are 0.1, 0.2, 0.5, 1.0, 2.0, and 3.0 (g kg^{-1}). The contour level for ice, snow, and hail is 0.1 g kg^{-1}.

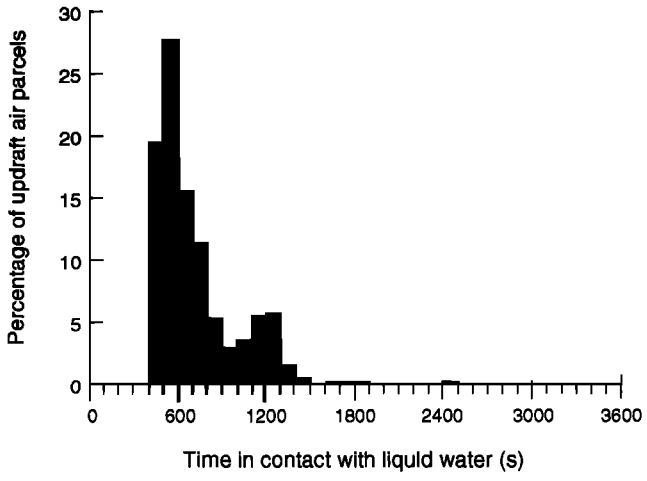

Figure 3. Histogram of parcel residence time in contact with liquid water in the updrafts. The updraft residence time is defined as the time it takes a parcel to rise from 4 km MSL to 0.5 km below the maximum altitude obtained along the trajectory. Time in contact with liquid water is the time during the updraft ascent that the air parcel was in contact with a total liquid water $(q_c + q_r) > 0.01$ g kg^{-1}.

evolved from a multicellular convective system to a supercellular system, as was observed. A comparison of simulated winds to Doppler analysis showed that the simulation generally captured both the speed and direction at most altitudes. In general, below 2 km MSL (0.5 km above ground level (AGL)) the flow was southeasterly. Between 2 and 3 km MSL the flow shifted to southwesterly and then westerly. Above 3.5 km MSL the flow was primarily from the northwest. The anvil, composed of snow and ice according to the simulation, had a northwest-southeast orientation. Figure 2 shows the orientation of the snow anvil at 11.5 km MSL at 3600 s and 9000 s in the simulation. At 3600 s the snow mixing ratio has three regions of high values, indicating the multiple cells. At 9000 s the snow mixing ratio illustrates a single cell and the anvil is aligned more in the west-east orientation.

Absorption of chemical species is assumed to occur in only the liquid phase and depends on the liquid water content at each grid point. Shown in Figure 2 are the mixing ratios of the cloud water and rain superimposed upon the location of the ice, snow, and hail fields at two times during the simulation, located along the AB and CD lines denoted in the x y cross section. At 3600 s the three cells are easily seen. Cloud water mixing ratios reach values > 0.5 g kg^{-1}. Rain mixing ratios reach values > 1.0 g kg^{-1}. Snow and hail play an important role in collecting cloud and rain drops. Snow is found primarily in the anvil region, with mixing ratios reaching values of > 3 g kg^{-1}. Hail is found mostly in the core of the storm, where mixing ratios are between 0.5 and 1.5 g kg^{-1}.

At 9000 s cloud water remains in the core of the cell, with mixing ratios reaching 2.5 g kg^{-1}. Rain mixing ratios are generally < 1.5 g kg^{-1}. There is an extensive snow anvil in which mixing ratios reach values up to 3.5 g kg^{-1}. Hail again is found mostly in the core of the storm, with mixing ratios reaching 7 g kg^{-1}.

Trajectories of air parcels that were released from the lowest 4 km above the surface along the cross section EF (Figure 2) at 30 min into the simulation were found to have reached convective updrafts between 70 and 90 min in the model

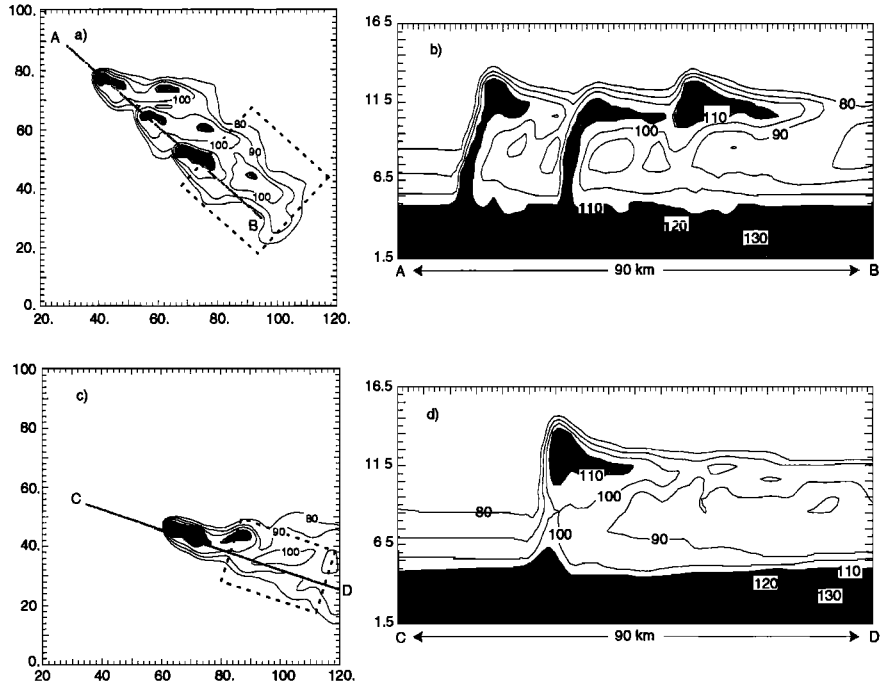

Figure 4. Passive tracer (C1) mixing ratios (ppbv) at (a) $t = 3600$ s and 11.5 km mean sea level, (b) $t = 3600$ s along the AB cross section (c) $t = 9000$ s and 11.5 km MSL, and (d) $t = 9000$ s along the CD cross section.

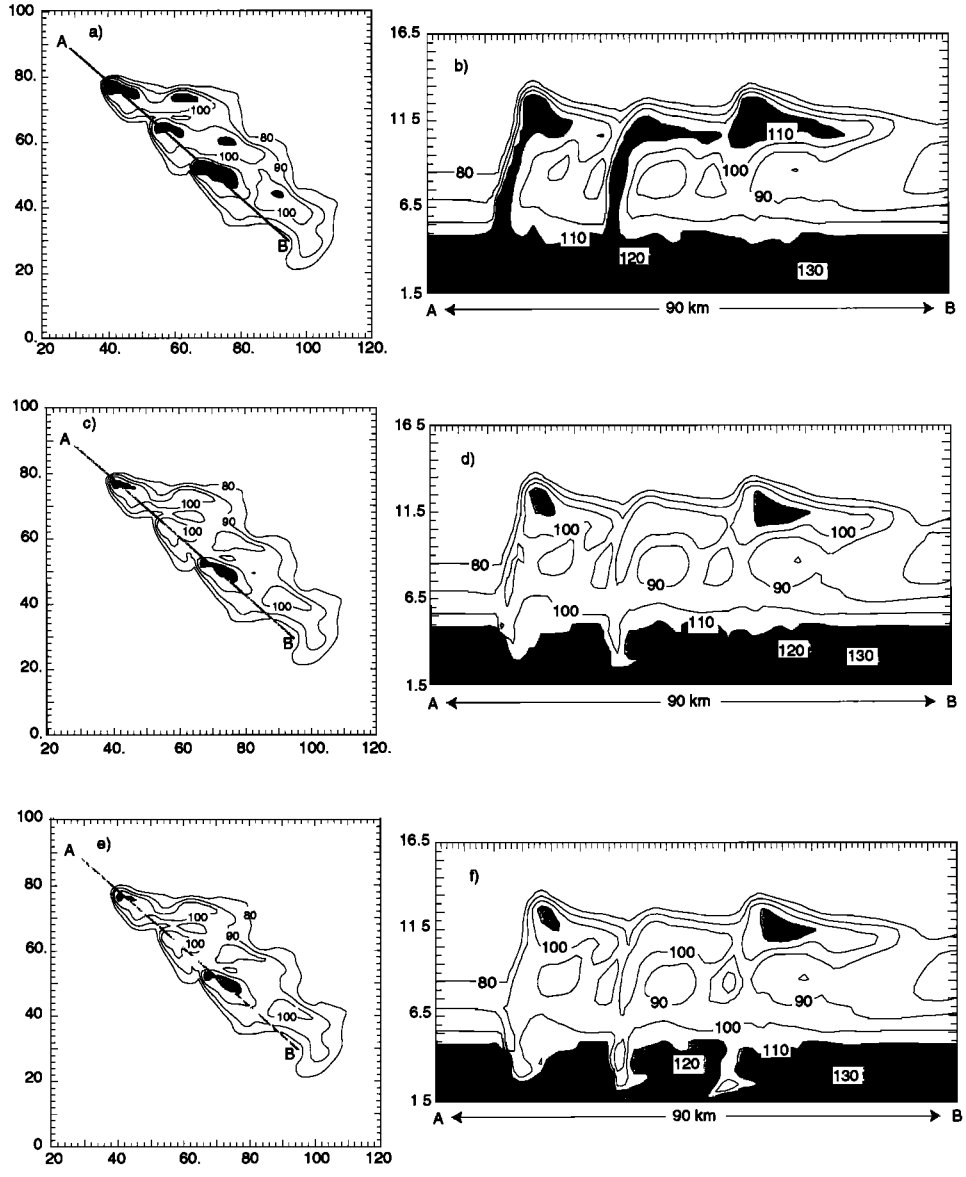

Figure 5. Soluble tracer (C10) mixing ratios (ppbv) at t = 3600 s for the simulation in which the soluble tracer is degassed when liquid drops are converted to ice, snow, or hail (a) at 11.5 km MSL and (b) along the AB cross section. Soluble tracer (C15) mixing ratios (ppbv) at t = 3600 s for the same simulation (c) at 11.5 km MSL and (d) along the AB cross section. Soluble tracer (C18) mixing ratios (ppbv) at t = 3600 s for the same simulation (e) at 11.5 km MSL and (f) along the AB cross section.

simulation. *Skamarock et al.* [2000] found that air parcels that were released at and below 500 m above the surface did not reach their level of free convection. Instead, air parcels from 2.0 to 3.5 km MSL were ingested by the storm. A histogram of the residence time an air parcel spent in the updraft (defined as the time for a parcel to travel from 4.0 km MSL to 500 m below its maximum attained height) showed that 34% of the trajectories had a residence time in the updraft between 500 and 700 s and 75% of the updrafts had a residence time between 500 and 1200 s.

To determine what the typical length of time an air parcel is in contact with liquid water, the trajectories calculated by *Skamarock et al.* [2000] were analyzed by finding the length of time that the sum of the cloud water and rain mixing ratios was positive. A histogram of the time an air parcel is in contact with liquid water is shown in Figure 3. Most parcels (74%) spend between 400 and 800 s in contact with liquid water. Because the extent of the cloud water is only to 9.5 km MSL and the updrafts reach 14 km MSL, the residence time in contact with liquid water is a bit shorter than the residence time in the updraft that was found by *Skamarock et al.* [2000], and there is no appreciable tail to the frequency distribution. Timescales of 400–800 s are not large compared to the chemical lifetime of many species (e.g., O_3, NO_x, and many nonmethane hydrocarbons have chemical lifetimes of an hour or more [*Brasseur et al.*, 1999]), and the influence

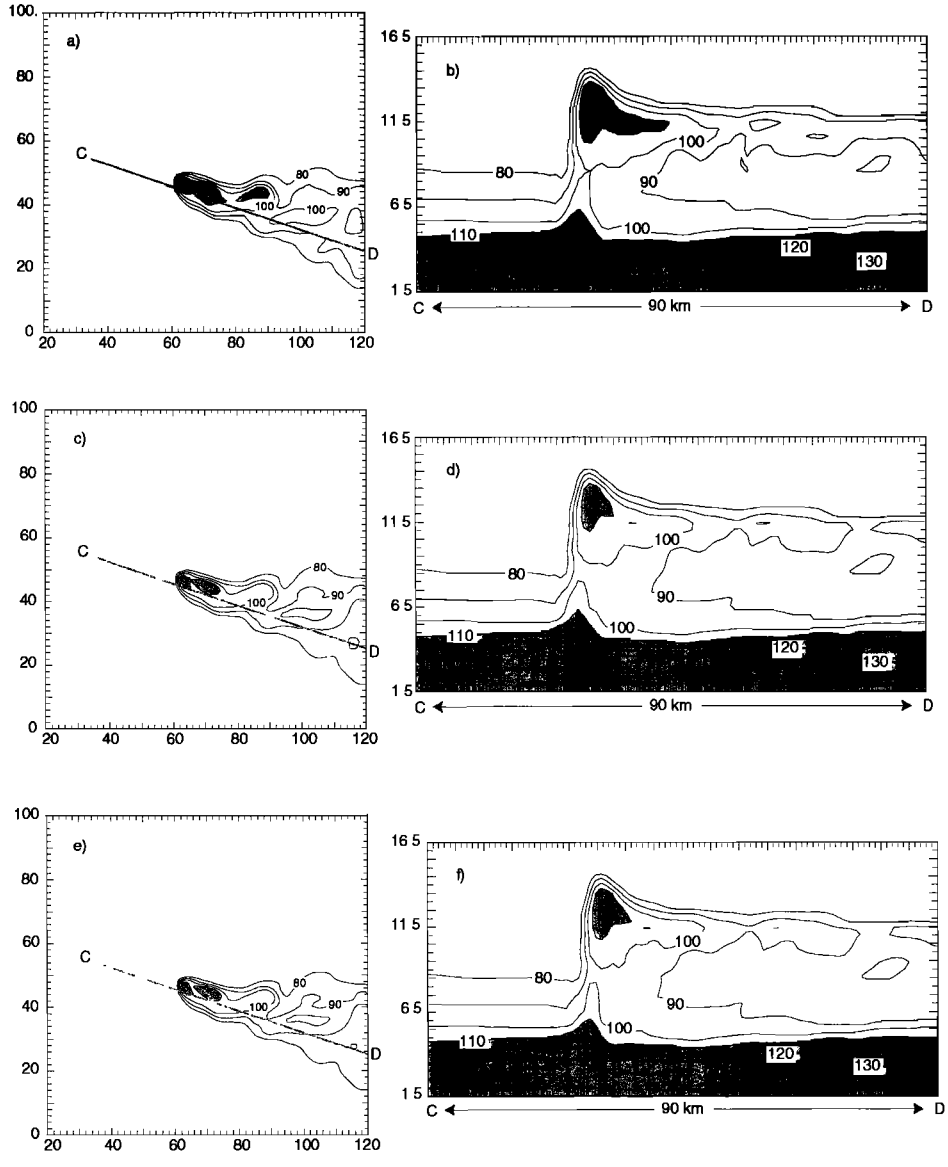

Figure 6. Same as Figure 5, except for t = 9000 s and for the CD cross section.

of the aqueous phase on the soluble species may not be significant.

3.2. Soluble Tracers That Are Degassed When Liquid Drops Are Converted to Frozen Particles

As discussed by *Skamarock et al.* [2000], the CO passive tracer is transported from the boundary layer where CO mixing ratios reach 135 ppbv to the anvil at ~ 10 km above the surface where CO mixing ratios exceed 110 ppbv (Figure 4). The distribution of the passive tracer can be used as a reference to the distributions of the soluble tracers. Because we examine snapshots of the chemical distributions during the storm's life, the total mixing ratio (sum of the mixing ratio in the gas phase, cloud water, and rain) of the soluble tracer is compared to the passive tracer. To exemplify differences between the distributions, only three tracers are discussed, C10 (K_H = 100 M atm^{-1}), C15 (K_H = 10^5), and C18 (K_H = 10^{12}). C10 has a solubility between acetone (K_H = 40 M atm^{-1}) and methyl hydrogen peroxide (K_H = 300 M atm^{-1}). C15 has a solubility similar to hydrogen peroxide, and C18 has a solubility similar to nitric acid.

Figure 5 illustrates the chemical distribution of C10, C15, and C18 at 1 hour into the simulation in which the soluble tracer is degassed when liquid drops are converted to ice, snow, or hail. There appears to be marked differences between the passive tracer distribution (Figure 4) and the highly soluble tracer distributions at t = 3600 s. In the anvil, mixing ratios of the passive tracer exceed 110 ppbv, while for the highly soluble tracers (C15 and C18), mixing ratios are generally between 100 and 110 ppbv. At t = 9000 s, there is a less noticeable difference between the passive or low-solubility tracers and the high-solubility tracers (Figure 6).

To quantify further the differences between the soluble

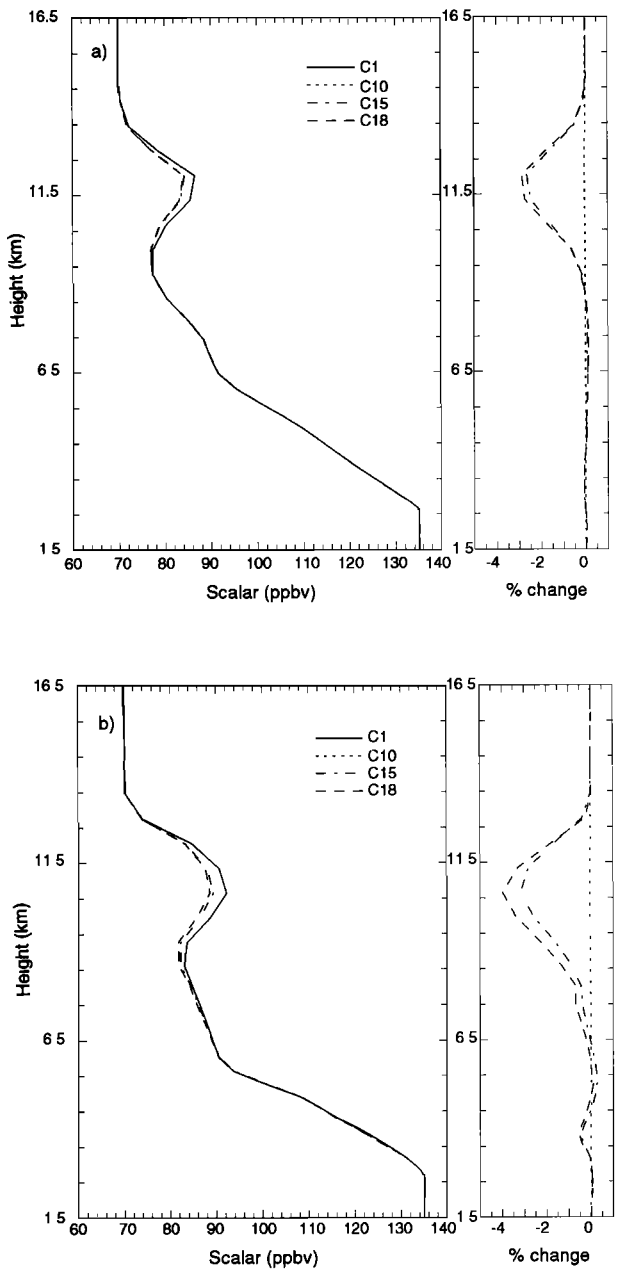

Figure 7. Average vertical profiles of the passive (C1) and soluble (C10, C15, and C18) tracers for the simulation in which the soluble tracers are degassed during conversion of liquid drops to ice, snow, or hail at (a) t = 3600 s in an area demarked by the x, y locations (68.1, 40.7), (91.4, 66.8), (117.4, 43.6), and (94.1, 17.5); and (b) t = 9000 s in an area demarked by the x, y locations (80.0, 28.0), (87.0, 49.0), (119.0, 38.3), and (112.0, 17.3). Also shown is percent change of the soluble tracers from the passive tracer.

tracers and the passive tracer, the average mixing ratios are calculated for a region (marked in Figure 4) in the outflow of the storm. These results are dependent on the size of the region. Clearly, as the size of the region increases to include areas of undisturbed air, small perturbations from the passive tracer would be found. However, the relative differences between soluble and passive tracers should still be apparent. We find that the average total mixing ratios in the outflow region of the storm show small differences between the soluble tracers and the passive tracer (Figure 7) at both t = 3600 s and t = 9000 s. The anvil is the region that illustrates the greatest differences, but still there is < 5% difference between the average mixing ratio of the soluble tracers and the passive tracer.

3.3. Soluble Tracers Retained in Ice Particles

The chemical distribution of C10, C15, and C18 at 1 hour into the simulation is illustrated in Figure 8 for the simulation where the soluble tracers are retained in the frozen hydrometeors during conversion of liquid drops to ice, snow, or hail. There are substantial differences among the different soluble tracer distributions and the passive tracer distribution (Figure 4). Soluble tracer C10 (K_H = 100 M atm^{-1}) has a distribution similar to the passive tracer, with mixing ratios exceeding 100 ppbv in the anvil. Soluble tracers C15 (K_H = 10^5 M atm^{-1}) and C18 (K_H = 10^{12} M atm^{-1}) have much smaller mixing ratios in the anvil compared to C10 and the passive tracer. The anvil mixing ratios of C15 and C18 are also much smaller than the C15 and C18 mixing ratios for the simulation in which the soluble tracers were degassed during conversion of liquid drops to ice, snow, or hail (Figure 5). At t = 9000 s, lower mixing ratios of the highly soluble tracers C15 and C18 are found in the anvil (Figure 9), whereas C10 mixing ratios are similar to the passive tracer. Again, when C15 and C18 mixing ratios are compared from the simulation in which the soluble tracer is retained in the ice to those from the simulation in which the soluble tracer is degassed during conversion of liquid drops to ice, snow, or hail, the mixing ratios in the anvil region are much lower from the simulation in which the soluble tracer is retained in the ice.

Average total mixing ratios of the soluble tracers in the outflow region (marked in Figure 4) of the storm indicate that the highly soluble tracers (C15 and C18) are reduced by 40-60% compared to the passive tracer (C1) at both t = 3600 s and t = 9000 s (Figure 10). Again, these results depend upon the size of the averaging region; smaller differences would be found if more undisturbed air is included in the average. When compared to Figure 7, it is evident that for the simulation where the soluble tracers are retained in the ice hydrometeors during conversion of liquid drops to ice, snow, or hail, the highly soluble tracers are depleted to a much greater extent than the highly soluble tracers that were degassed during conversion of liquid drops to ice, snow, or hail.

The results found in Figures 7 and 10 imply that large-scale models for which deep convection is a subgrid parameterization may be overestimating the loss of highly soluble species in the upper troposphere. For example, *Crutzen and Lawrence* [2000] show mixing ratios of highly soluble species (K_H > 10^5 M atm^{-1}) in which the mixing ratios are 25% or less of the passive tracer in the mid-troposphere to upper troposphere. The results of *Crutzen and Lawrence* [2000] are monthly averages from a global model of ~

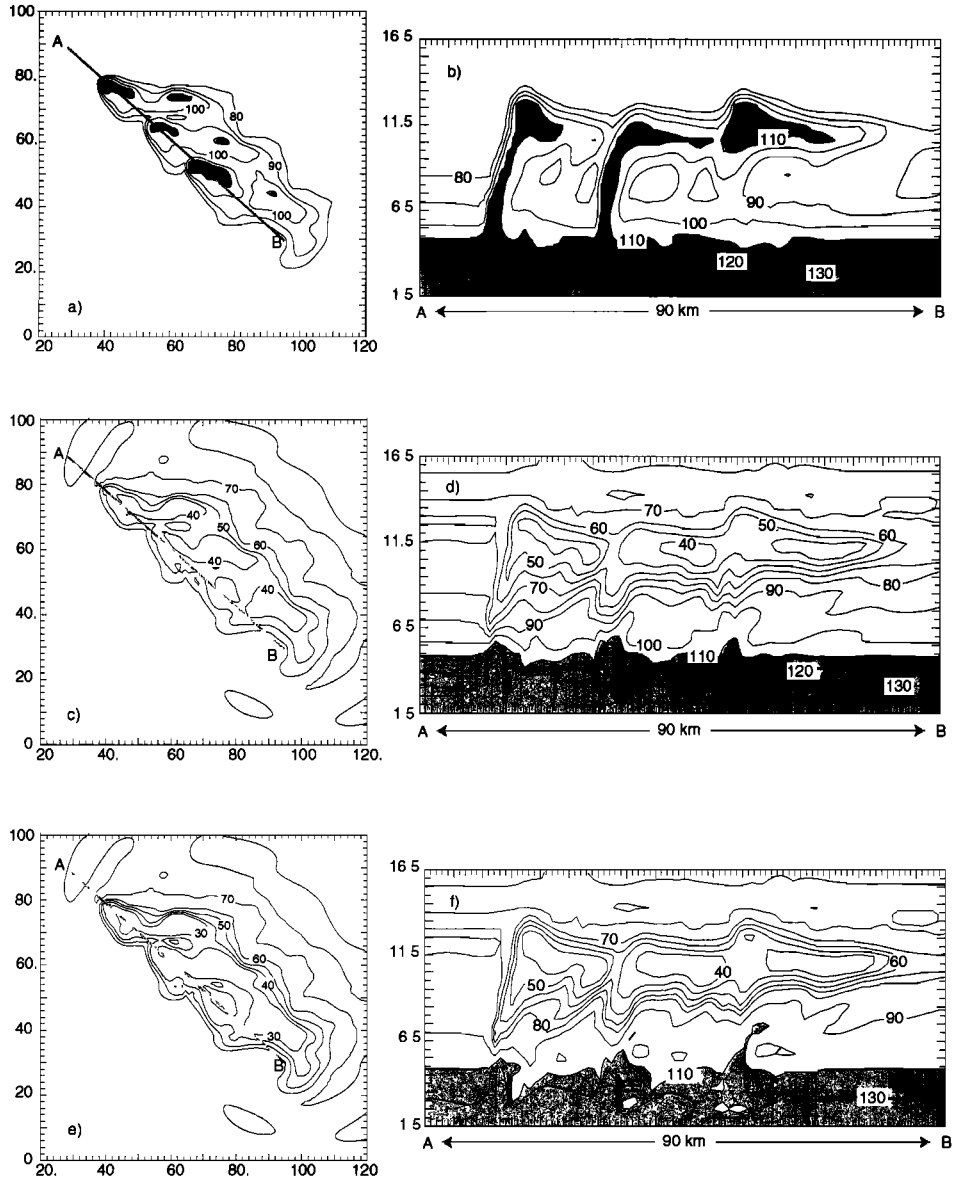

Figure 8. Soluble tracer (C10) mixing ratios (ppbv) at t = 3600 s for the simulation in which soluble tracers are retained in the ice (a) at 11.5 km MSL and (b) along the AB cross section. Soluble tracer (C15) mixing ratios at t = 3600 s for the same simulation (c) at 11.5 km MSL and (d) along the AB cross section. Soluble tracer (C18) mixing ratios at t = 3600 s for the same simulation (e) at 11.5 km MSL and (f) along the AB cross section.

2° horizontal resolution. Thus their results include many convective events (both temporally and spatially) and cannot be directly compared to our results. However, our results show the importance of entrainment of the environmental background air into the anvil region. Sensitivity studies with our cloud model indicate that if the initial profile were assumed to have very little or no concentration of the tracer in the mid-troposphere to upper troposphere, greater depletion in the anvil region of the soluble tracers would occur. Last, our results may differ from what is shown in Figures 7 and 10 if a different size region were used for the analysis; larger regions would contain more undisturbed air, thus reducing the impact of the convection on upper tropospheric concentrations.

3.4. Sources and Sinks of Soluble Tracers

As outlined in section 2.2, the tendency equation of the soluble tracer includes the transfer of the tracer from one hydrometeor field to another. In this section we contrast the sources and sinks of the tracers for the simulation where the tracer is degassed when liquid drops are converted to ice, snow, or hail and the simulation where the tracer is retained in the frozen hydrometeors.

Figure 11 illustrates the horizontal sum of the sources and sinks affecting C10 in cloud water and C18 in cloud water during the multicellular stage of the storm (t = 3600 s) and during the quasi-supercellular stage of the storm (t = 9000 s) for the simulation where the tracer is degassed

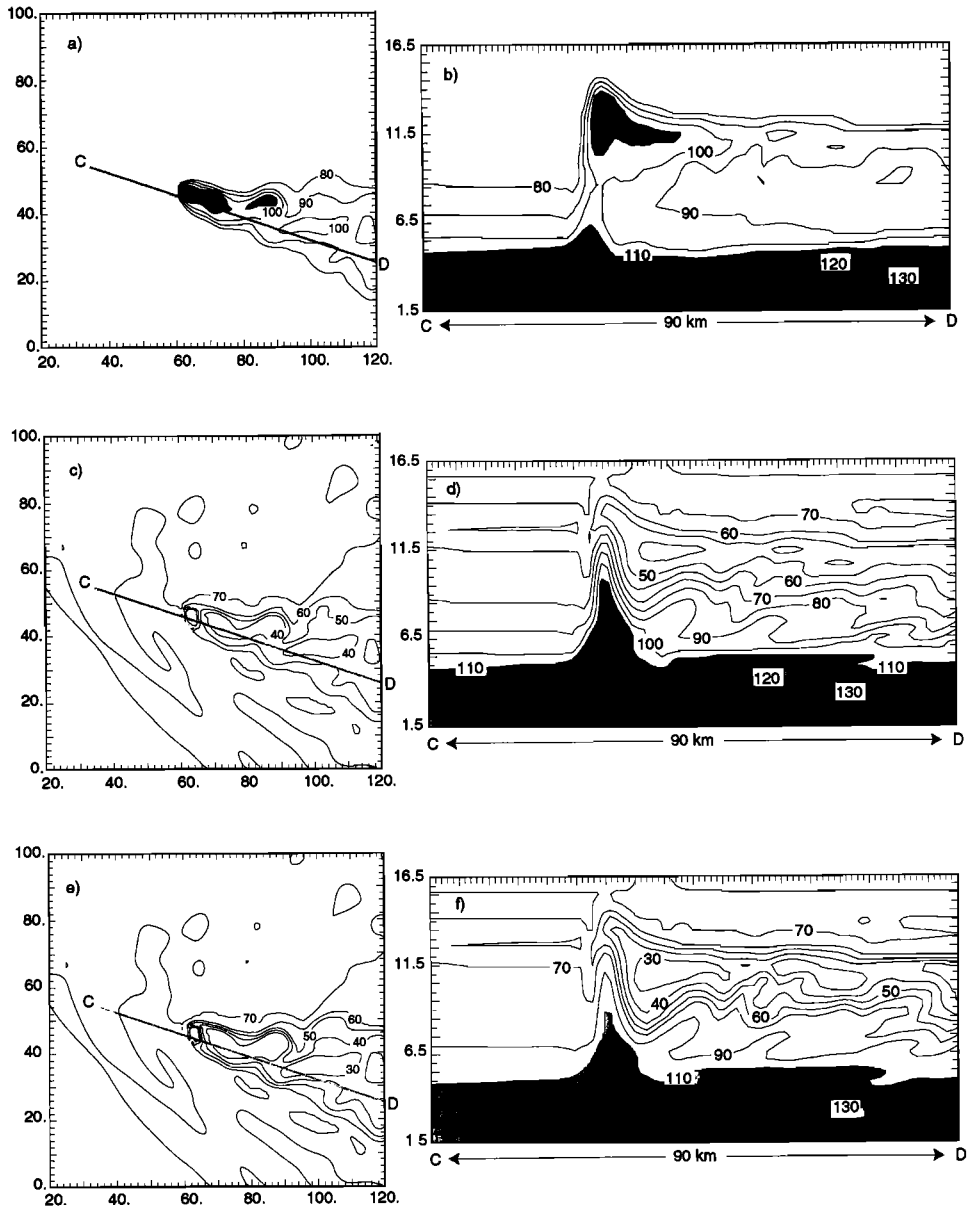

Figure 9. Same as Figure 8, except for $t = 9000$ s and along the CD cross section.

during conversion of liquid drops to ice, snow, or hail. The source of the tracer in the cloud water is the absorption of the tracer from the gas phase. For C10 this source is largest in the lower portion of the cloud and decreases with height. At $t = 3600$ s the transfer of C10 to rain via accretion and autoconversion occurs primarily in the lower regions of the core of the storm. From $z = 4$ km MSL and higher, C10 is degassed when the cloud water is collected by snow and hail. At $t = 9000$ s, transfer of C10 from cloud water to rain occurs through a greater depth of the lower portion of the storm core. However, C10 is still primarily removed via degassing during accretion of cloud water by snow and hail.

At both times shown, C18 has two peaks for absorption of C18 from the gas phase into the cloud water. The first peak occurs near cloud base ($z = 3.5$ km MSL) where both cloud water mixing ratios and C18 mixing ratios are high. The second peak is broadly distributed from 5 to 9.5 km MSL. The sink of C18 in cloud water maximizes in this same region. This indicates that once C18 is degassed when snow and hail collect cloud water, C18 is readily absorbed into the remaining cloud water in the region.

When the soluble tracers are retained in the frozen hydrometeor, the sources and sinks for C10 are not altered substantially (Figure 12). However, instead of C10 being transferred to the gas phase, it is transferred to snow and hail at middle to upper regions of the storm. In addition, there is a small source to ice when the cloud water freezes homogeneously at temperatures below -40°C.

There is still a large source of C18 in cloud water near cloud base via the absorption of C18 from the gas phase, but the secondary peak in the middle to upper regions of the storm is diminished, because there is little C18 in the gas

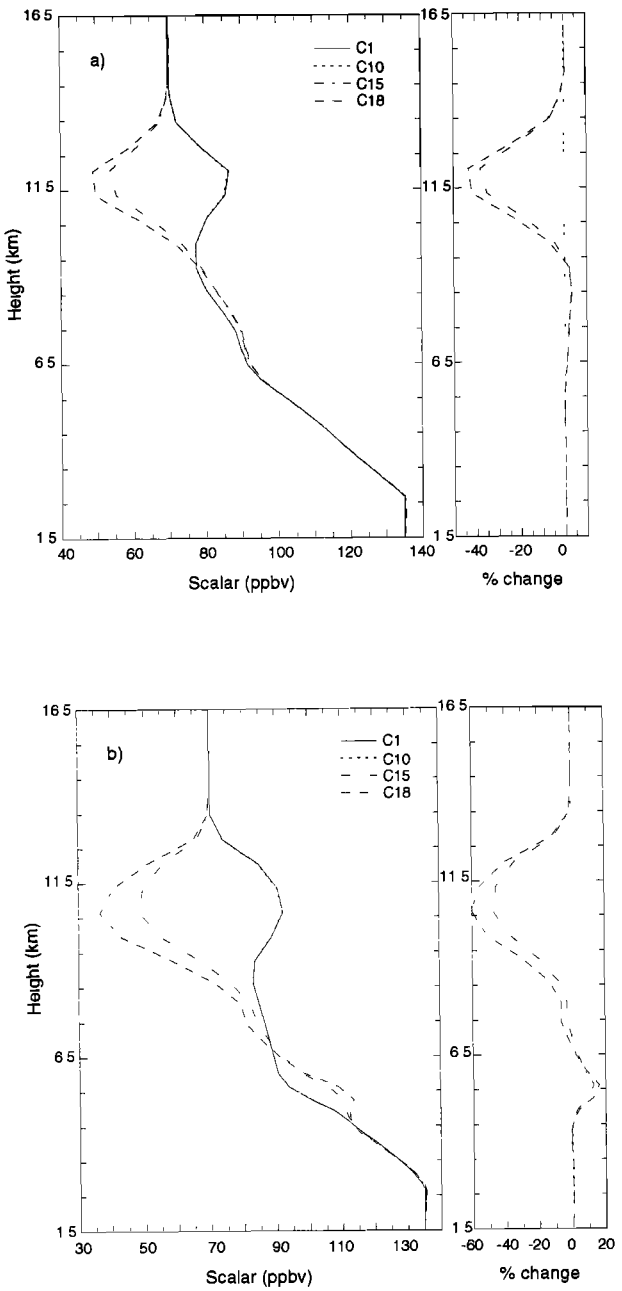

Figure 10. Average vertical profiles of the passive (C1) and soluble (C10, C15, and C18) tracers for the simulation in which the soluble tracers are retained in the ice during conversion of liquid drops to ice, snow, or hail at (a) t = 3600 s in an area demarked by the x, y locations (68.1, 40.7), (91.4, 66.8), (117.4, 43.6), and (94.1, 17.5) and (b) t = 9000 s in an area demarked by the x, y locations (80.0, 28.0), (87.0, 49.0), (119.0, 38.3), and (112.0, 17.3). Also shown is percent change of the soluble tracers from the passive tracer.

phase in this portion of the storm. The other thing to note is that the magnitude of the sources and sinks of C18 in cloud water is much smaller for the simulation where the tracer is retained in the frozen hydrometeors than for the simulation where the tracer is degassed during conversion of liquid drops to ice, snow, or hail. This reflects the lower mixing ratios of C18 within the storm, since more C18 is precipitated by snow and hail out of the region.

Once the soluble tracer becomes part of the snow or hail, it continues to be advected by the air motions, fall by sedimentation, and be transferred via microphysical processes. The sources and sinks of C18 in snow indicate that much of the tracer is transferred to hail via the collection of snow by hail and that a smaller portion of C18 is transferred to rain via melting (especially at t = 3600 s). The hail precipitates and C18 is transferred from hail to rain through melting. This is a very large sink of C18, which indicates that much of the tracer is deposited to the ground.

4. Discussion

4.1. Net Flux of Soluble Tracers

The conservation equation for the total mixing ratio of a soluble tracer can be expressed as

$$\frac{\partial(\bar{\rho}C_{\text{tot}})}{\partial t} = -\frac{\partial(\bar{\rho}uC_{\text{tot}})}{\partial x} - \frac{\partial(\bar{\rho}vC_{\text{tot}})}{\partial y} - \frac{\partial(\bar{\rho}wC_{\text{tot}})}{\partial z} + \frac{\partial[\bar{\rho}\sum_{n=1}^{3}(V_{p,n}f_nC_{\text{tot}})]}{\partial z}, \quad (15)$$

where C_{tot} (= $C_{\text{gas}} + C_{cw} + C_r + C_i + C_s + C_h$) is the total mixing ratio of the tracer, $V_{p,n}$ is the precipitation fall speed for precipitation hydrometeor n (rain, snow, and hail), and f_n is the fraction of C_{tot} that resides in each of the precipitation hydrometeors. Following *Skamarock et al.* [2000], the convective vertical transport can be determined by horizontally integrating (15) over the domain.

$$\frac{\partial}{\partial t}\int_{\Omega}(\bar{\rho}C_{\text{tot}})\,\partial\Omega = -\int_{\Gamma}(\bar{\rho}u_nC_{\text{tot}})\,\partial\Gamma - \int_{\Omega}\left[\frac{\partial(\bar{\rho}wC_{\text{tot}})}{\partial z} - \frac{\partial[\bar{\rho}\sum_{n=1}^{3}(V_{p,n}f_nC_{\text{tot}})]}{\partial z}\right]\partial\Omega. \quad (16)$$

Equation (16) gives the instantaneous change in the tracer mass at a height z, horizontally integrated over the domain Ω with spatial boundaries Γ and boundary-normal velocity u_n. *Skamarock et al.* [2000] found that the first term on the right-hand side of the equation, i.e., the net flux through the boundaries, is always much smaller than the other terms and can therefore be neglected. The second term on the right-hand side of (16) represents the horizontally integrated advective vertical flux divergence, while the last term represents the horizontally integrated precipitative vertical flux divergence.

The vertical flux divergence of the tracer as a function of height can be found when (16) is integrated over time,

$$\int_0^t\int_{\Omega}\frac{\partial}{\partial z}\left[\bar{\rho}wC_{\text{tot}} - \bar{\rho}\sum_{n=1}^{3}(V_{p,n}f_nC_{\text{tot}})\right]\partial\Omega\,\partial t. \quad (17)$$

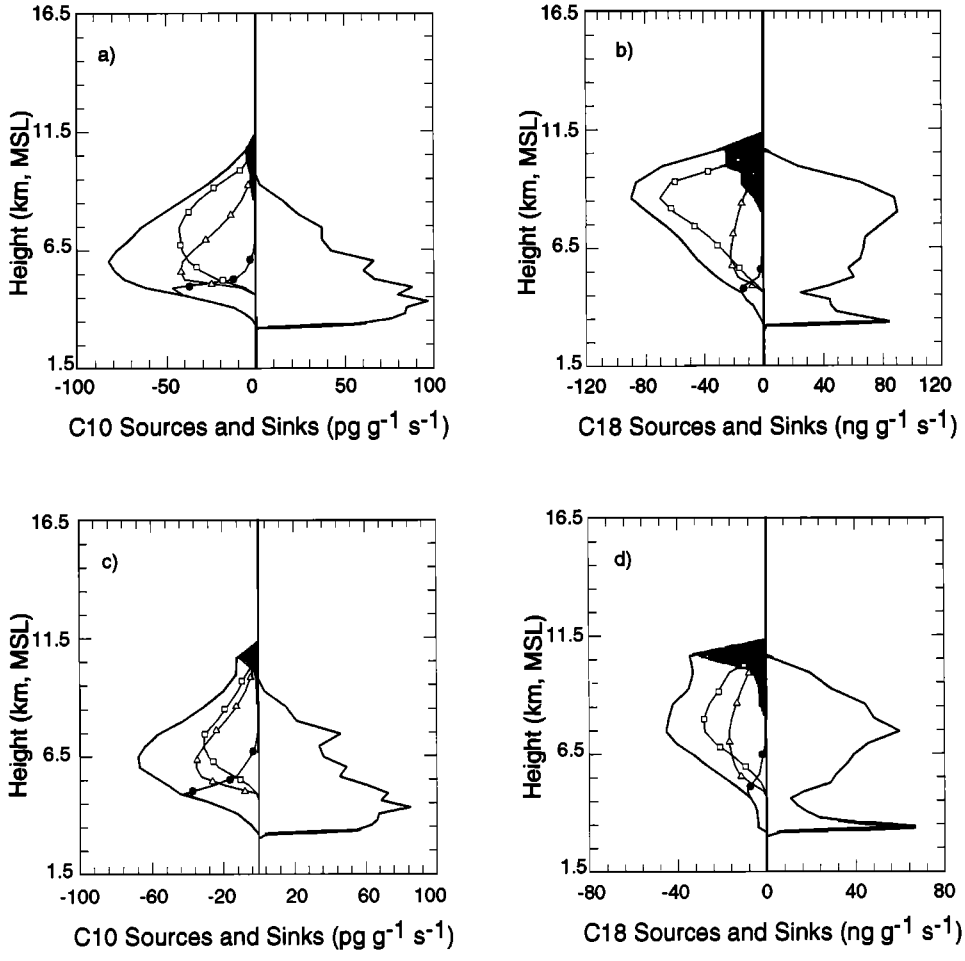

Figure 11. Vertical profiles of the horizontal sum of the sources and sinks for the simulations where the soluble species degasses during conversion of liquid drops to ice, snow, or hail of (a) C10 in cloud water at t = 3600 s, (b) C18 in cloud water at t = 3600 s, (c) C10 in cloud water at t = 9000 s, and (d) C18 in cloud water at t = 9000 s. Thick lines are the mass transfer of the tracer from gas phase to cloud water (positive values) and the total loss of the tracer from cloud water via microphysical processes. The solid line marked with squares indicates the transfer of the tracer from the cloud water to gas via snow accretion of cloud water. The solid line marked with triangles indicates the transfer of the tracer from the cloud water to gas via hail accretion of cloud water. The solid line marked with solid circles indicates the transfer of cloud water to rain through accretion and autoconversion processes. The shaded region indicates the transfer of the tracer from the cloud water to gas via conversion of cloud water to ice.

An insoluble tracer, such as C1, is affected by only the vertical advective flux divergence while a soluble tracer is affected by both the advection and the precipitation. The vertical flux divergence for the insoluble tracer (C1) is the same as that found by *Skamarock et al.* [2000] for their passive CO tracer for the same storm (Figure 13). Throughout the simulation it is found that the insoluble tracer is advected from the lower levels of the storm to above 8 km MSL.

The 3-hour time-integrated total vertical flux divergence for C10, C15, and C18 shows the influence of precipitation, particularly snow and hail, upon the soluble tracers (Figure 13). C10 is not affected by the precipitation for either simulation. For the simulation in which the species is degassed during conversion of liquid drops to ice, snow, or hail, the precipitative flux divergence for C15 and C18 affects the total vertical flux divergence below 5.5 km MSL only. The precipitative flux divergence for this simulation is small and enhances the negative vertical flux divergence near 4 km MSL and near the surface. Because the cloud water does not have an appreciable fall speed, the species in the cloud water is advected in the same manner as the passive tracer is advected in the gas phase. Thus the total vertical flux divergence is nearly the same for all tracers.

For the simulation in which the species is retained in the ice during conversion of liquid drops to ice, snow, or hail, the precipitative flux divergence for C15 and C18 removes the tracer from the region above 5.5 km MSL to the region below this level. This removal counteracts the advective flux divergence, which is transporting the soluble tracer in the cloud water, hail, and snow to above 5.5 km MSL, resulting in a total vertical flux divergence of no gain and a little loss above 8 km MSL. The fact that the highly soluble tracer (C18) illustrates some loss in the anvil region indicates that the precipitative flux divergence is removing some environ-

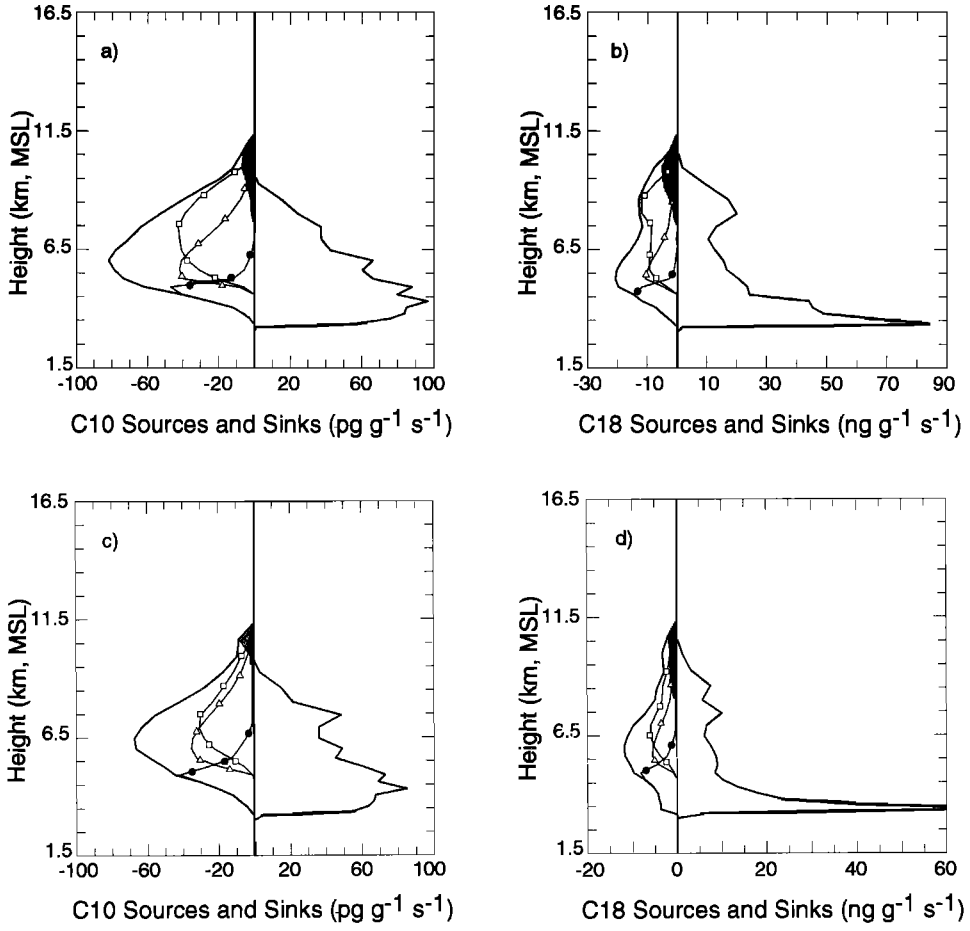

Figure 12. Vertical profiles of the horizontal sum of the sources and sinks for the simulation where the soluble tracers are retained in the ice during conversion of liquid drops to ice, snow, or hail of (a) C10 in cloud water at t = 3600 s, (b) C18 in cloud water at t = 3600 s, (c) C10 in cloud water at t = 9000 s, and (d) C18 in cloud water at t = 9000 s. Thick lines are the mass transfer of the tracer from gas phase to cloud water (positive values) and the total loss of the tracer from cloud water via microphysical processes. The solid line marked with squares indicates the transfer of the tracer from the cloud water to snow via snow accretion of cloud water. The solid line marked with triangles indicates the transfer of the tracer from the cloud water to hail via hail accretion of cloud water. The solid line marked with solid circles indicates the transfer of cloud water to rain through accretion and autoconversion processes. The shaded region indicates the transfer of the tracer from the cloud water to ice during freezing and through the Bergeron process.

mental, upper tropospheric soluble tracer that has been entrained into the anvil region.

The net flux divergence of the soluble tracers in the 8- to 15-km region is shown as a function of time in Figure 14. For the simulation where the soluble tracer is degassed during conversion of liquid drops to ice, snow, or hail, the precipitative flux divergence contributes negligibly to the net flux divergence throughout the integration of the simulation. This is also true when the flux divergence is temporally integrated (Figure 14b). Thus the change in mass in the 8- to 15-km MSL region is due to the advective flux divergence of the soluble tracer for the simulation where the soluble tracer is degassed during conversion of liquid drops to ice, snow, or hail.

For the simulation where the soluble tracer is retained in the ice during conversion of liquid drops to ice, snow, or hail, the precipitative flux divergence reduces the net flux divergence for the highly soluble tracers (Figure 14c). The precipitative flux divergence for this simulation is largest during the early stages of the multicellular phase (t = 30 min) and during the mature phase of the quasi-supercellular stage (t = 3 hours) of the storm. The temporally integrated precipitative flux divergence (Figure 14d) for the highly soluble tracers (C15 and C18) offsets the advective change of the soluble tracer in the 8- to 15-km region. This results in essentially no change in the mass of C15 and a net loss of C18 in the 8- to 15-km region throughout the simulation.

4.2. Scavenging Efficiencies of Soluble Tracers

Different methods have been used to define and calculate the scavenging efficiency of a storm during the past few decades. One method is to define a scavenging coefficient as the first-order removal rate of a species by the storm. Many

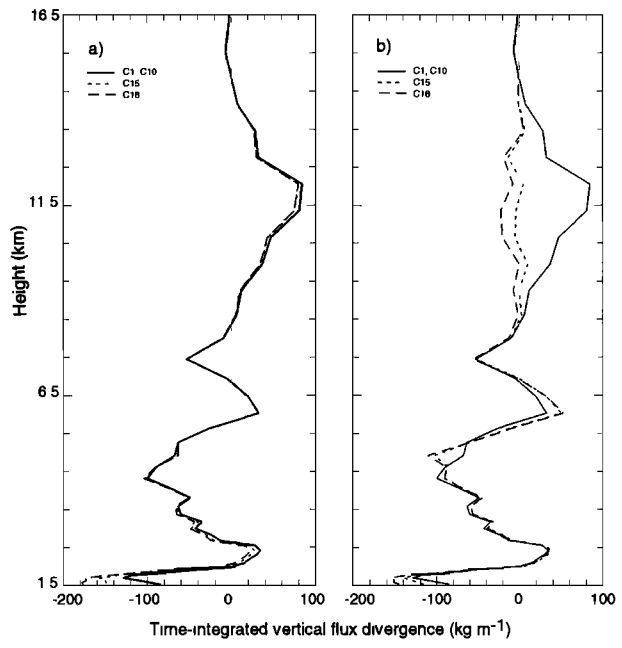

Figure 13. Time-integrated total flux divergence for the tracers at 3 hours for (a) the simulation in which the soluble tracers are degassed during conversion of liquid drops to ice, snow, or hail and (b) the simulation in which the soluble tracers are retained in the ice during conversion of liquid drops to ice, snow, or hail.

large-scale models that include a washout parameterization for soluble species employ a first-order removal mechanism [*Giorgi and Chameides*, 1986].

A second method is to define a washout ratio as the concentration of a species in the precipitation to the concentration of the species in the inflow air of the storm. To perform this calculations, many experimentalists have assumed that the concentration of the species in the inflow air can be estimated from the concentration at the ground station.

Easter and Hales [1983] defined a wet removal efficiency as the ratio of the wet deposition flux of the species to the flux of the species transported into the storm. From their two-dimensional cloud simulations, they found that nitric acid had a wet removal efficiency of 0.92.

Cohan et al. [1999] determined the scavenging efficiency of convection on a soluble species using a two-component mixture method. Using an insoluble tracer, they first determined the dilution factor as

$$\beta = \frac{X_{\mathrm{BL}} - X_{\mathrm{conv}}}{X_{\mathrm{BL}} - X_{\mathrm{UT}}}, \tag{18}$$

where X is the mixing ratio of the insoluble species in the boundary layer (BL), the convectively influenced air (conv), and the upper troposphere (UT). The scavenging efficiency α can then be found from β and the soluble species mixing ratio Y,

$$\alpha = 1 - \frac{Y_{\mathrm{conv}} - \beta Y_{\mathrm{UT}}}{(1-\beta)\, Y_{\mathrm{BL}}}. \tag{19}$$

If one has measurements of insoluble and soluble species in the boundary layer, convectively influenced air, and the undisturbed upper troposphere, then the scavenging efficiency of the soluble species can be determined. *Cohan et al.* [1999] found the scavenging efficiency of hydrogen peroxide to range from 55-70%. One difficulty with this method is accurately determining a representative mixing ratio for each of the regions, especially the convectively influenced region. The reason for this is that greater entrainment occurs near the edges of the convectively influenced region, while little or no entrainment occurs in the core of the region.

On the other hand, one can attempt to determine how much of a species should reach the upper troposphere, given the boundary layer mixing ratio of the soluble species and the scavenging efficiency. *Mari et al.* [2000] found from their one-dimensional cloud model that 5% of methyl hydrogen peroxide, 66% of the hydrogen peroxide, and 77% of the nitric acid was scavenged by deep convection.

We calculate the scavenging efficiency for the July 10, 1996, storm for the soluble tracers that were depicted by the three-dimensional simulations using the two-component mixture method outlined by *Cohan et al.* [1999] and the method used by *Easter and Hales* [1983]. For the two-component mixture method we use 133 ppbv for the boundary layer mixing ratio for both the insoluble and soluble tracers and 70 ppbv for the undisturbed upper tropospheric mixing ratio for both the insoluble and soluble tracers. The convectively influenced mixing ratios, listed in Table 2, are determined by averaging the mixing ratios in the outflow region (depicted by the dashed-line box in Figure 4 at 9000 s and averaged vertically from 9.5 to 14 km MSL).

For the scavenging efficiency calculation determined as the ratio of the wet deposition flux to the flux into the storm, we determine the flux into the storm by vertically integrating the vertical flux divergence from 2.0 to 3.1 km for just the updraft regions. These vertical levels are chosen based on the trajectory information examined by *Skamarock et al.* [2000]. The vertical flux divergence values are then integrated in time to the end of the simulation. Likewise, the wet deposition flux to the surface is integrated in time to the end of the simulation. Results from the scavenging efficiency calculations are listed in Table 2.

Both methods indicate > 50% scavenging of tracers with a solubility $> 10^5$ M atm^{-1} and < 5% scavenging of tracers with a solubility < 1000 M atm^{-1}. In general, scavenging efficiencies from the two-component mixture technique are $\sim$ 1.5 times greater than the flux method calculation. The shortcomings of the two-component mixture method are noted with the highly soluble tracers where the two-component mixture method indicates more than 100% of the tracer is scavenged.

4.3. Henry's Law Equilibrium

Many model parameterizations of wet deposition of species assume that the soluble species is in Henry's law equilibrium between the gas and aqueous phases. This assumption would seem to be valid for time steps greater than a few minutes,

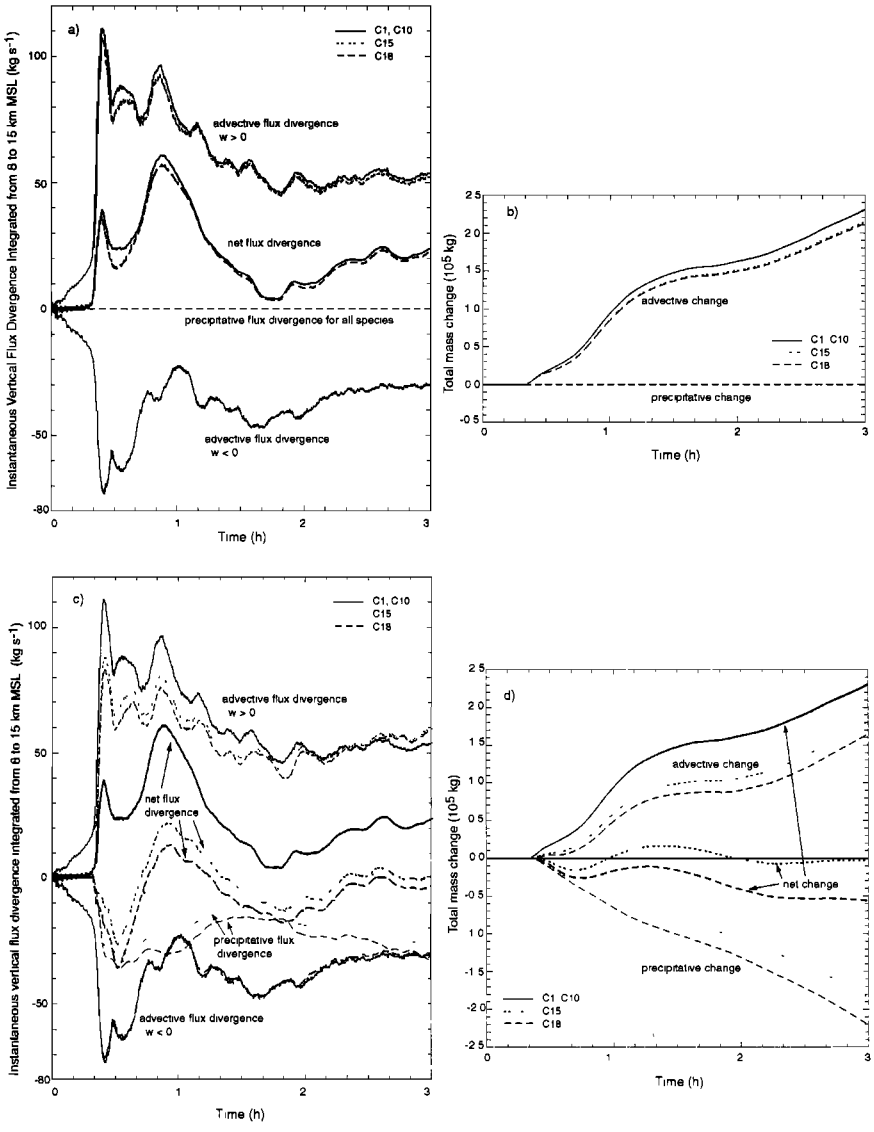

Figure 14. Vertical flux divergence integrated from 8- to 15-km MSL for (a) instantaneous values for the simulation in which the soluble tracers are degassed during conversion of liquid drops to ice, snow, or hail; (b) time-integrated values for the same simulation; (c) instantaneous values for the simulation in which the soluble tracers are retained in the ice during conversion of liquid drops to ice, snow, or hail; and (d) time-integrated values for the same simulation. The precipitative change for C1 and C10 in Figure 14d is essentially zero.

even for HNO_3, because this highly soluble species would be nearly in equilibrium (at least 90%) for such a large time step.

Using a 6-s time step and the method outlined in section 2.2.1, our results indicate that tracers with a solubility $< 10^3$ M atm^{-1} are in Henry's law equilibrium, while tracers with a solubility between 10^3 and 10^5 M atm^{-1} are in Henry's law equilibrium for the cloud drops but not the rain drops. Tracers with even higher solubilities are not in Henry's law equilibrium, and therefore the results for the highly soluble tracers may be sensitive to the size of the drops, which was prescribed for cloud drops and diagnosed for rain drops in the simulations performed for this study.

4.4. Implications for H_2O_2, CH_3OOH, and $CH_3C(O)CH_3$

It has been hypothesized that deep convection may be affecting the odd hydrogen (HO_x) budget in the upper troposphere [*Prather and Jacob*, 1997; *Jaeglé et al.*, 1997]. *Jaeglé et al.* [1997], using aircraft data, found, on occasion, higher concentrations of HO_x in the upper troposphere that could not be explained by local photochemistry. They surmised that deep convection, which occurred 3-5 days before the measurements were obtained, transported high values of peroxides, formaldehyde, and possibly acetone from the boundary layer to the upper troposphere. *Prather and Jacob* [1997] determined that the transport of methyl hydrogen peroxide

Table 2. Scavenging Efficiencies of the Soluble Tracers

Henry's Law Constant, M atm^{-1}	Deposition Flux to Flux Into Storm, %	Two-Component Mixture Model, %	Convectively Influenced Mixing Ratio, ppbv
0.001	0	0	88.0
0.01	0	0	88.0
0.1	0	0.3	87.9
1.0	0	0.3	87.9
5.0	0	0.3	87.9
10.	0	0.3	87.9
50.	0.2	0.5	87.8
100.	0.4	0.5	87.8
500.	2	3	87.0
1000.	3	5	86.1
5000.	13	21	80.2
10^4	22	34	75.1
10^5	55	86	55.2
10^6	69	100	47.6
10^7	72	100	46.0
10^{12}	72	100	46.0

by deep convection accounted for half the source of HO_x in the upper troposphere. With our cloud model we can assess how deep convection processes HO_x precursors, such as CH_3OOH, H_2O_2, CH_2O, and acetone. All of these species have some degree of solubility, so that they may be susceptible to scavenging. Furthermore, CH_3OOH, H_2O_2, and CH_2O concentrations may be modified by reactions in the liquid drops.

If we consider just the transport and solubility of chemical species in and near a deep convective storm, then from the simulations performed here we find that a species such as acetone ($K_H \sim 40\ M\ \text{atm}^{-1}$) or methyl hydrogen peroxide ($K_H \sim 300\ M\ \text{atm}^{-1}$) is readily transported to the upper troposphere. However, methyl hydrogen peroxide is reactive in liquid drops, so that it may experience some depletion due to aqueous chemistry. More soluble species, such as hydrogen peroxide and nitric acid, may have a substantial fraction scavenged when the entrapment of chemical species into ice during the conversion of liquid drops to ice, snow, or hail is considered. For hydrogen peroxide it has been observed that only a fraction is retained in the snow during riming [*Snider et al.*, 1992], thus the scavenging of hydrogen peroxide may not be as substantial as indicated in this study. Furthermore, for clouds that do not have a significant amount of ice, snow, or graupel, the simulation where the species are degassed during conversion of liquid drops to ice, snow, or hail indicates that all soluble tracers, including the highly soluble tracers, are transported to the middle to upper troposphere.

5. Conclusions

We use a three-dimensional convective cloud model to examine the chemical redistribution of tracers of varying solubility by deep convection. The convective cloud model simulation reasonably represents the structure and dynamics observed for the July 10, 1996, STERAO-Deep Convection storm [*Skamarock et al.*, 2000]. We examine the redistribution of soluble tracers for two cases, one in which the dissolved tracer is degassed during conversion of liquid drops to ice, snow, or hail and a second in which the dissolved tracer is retained in the ice during conversion of liquid drops to ice, snow, or hail. The results show that tracers of all solubilities are primarily transported to the upper troposphere when soluble tracers are degassed. Low-solubility tracers reside mostly in the gas phase and are transported to the upper troposphere. High-solubility tracers, present in the gas and cloud water, are primarily transported to the upper troposphere, although a small fraction is rained out. When retention is considered, only the low-soluble tracers remain primarily in the gas phase and are transported upward, similar to the transport of a passive tracer. The highly soluble tracers ($K_H \geq 10^5\ M\ \text{atm}^{-1}$) are retained in the snow and hail and are ultimately rained out. The key microphysical processes that dictated these results are accretion of cloud water by snow and hail.

Because of the entrainment process, consideration of the spatial scale is important to the amount of soluble tracer found in the anvil. The largest depletion in the anvil was noted on the few kilometer scale. On scales of $30 \times 30\ \text{km}^2$ the depletion was reduced by 10–20%. Because large-scale models have coarse resolution, the parameterization of convective transport and wet deposition of soluble species needs to be carefully evaluated with both field measurements and cloud-scale model results.

Another important aspect of this storm is the short residence time of air parcels in the updraft (500-800 s) com-

pared to chemical lifetimes and the shorter residence time in contact with liquid water (400-700 s). This could reduce the effect of solubility or mass transfer between gas and aqueous phases. Thus the scavenging efficiency for tracers with a Henry's law coefficient of 10^5 M atm^{-1} and higher may increase in storms that have a longer residence time in contact with liquid water.

Further consideration needs to be given to microphysical parameterizations. Bulk water microphysics parameterizations that depict the ice phase are highly parameterized for processes such as the formation of graupel/hail from riming. Thus the results presented here may be sensitive to the partitioning between ice and liquid hydrometeors, as depicted by the assumptions in the microphysics parameterization.

As we recognize the potential importance of certain chemical species (e.g., methyl hydrogen peroxide, hydrogen peroxide, and acetone) in the upper troposphere and realize that convection and frontal lifting are the main pathways for transporting these species to the upper troposphere, it is clear that we need to understand the processes that affect key species when they are exposed to cloud systems. This study shows that entrapment of highly soluble species by ice hydrometeors increases the scavenging of that tracer. However, few field experiments have examined the importance of the ice phase on chemical species, even though it appears that this information is crucial.

Clouds can affect chemical species distributions by processes other than transport, dissolution, microphysics, and washout. Aqueous-phase chemistry, adsorption of species onto ice particles, reactions on ice, and modified photolysis rates should also be considered.

Acknowledgments. A. L. Stuart was supported by a National Science Foundation graduate fellowship and a U. S. Environmental Protection Agency STAR Graduate Fellowship. W. C. Skamarock is partially supported under the NOAA Climate and Global Change Program award NA76GP00400. The National Center for Atmospheric Research is sponsored by the National Science Foundation.

References

Borys, R. D., P. J. Demott, E. E. Hindman, and D. Feng, The significance of snow crystal and mountain-surface riming to the removal of atmospheric trace constituents from cold clouds, in *Precipitation Scavenging, Dry Deposition, and Resuspension*, edited by H. R. Pruppacher, R. G. Semonin, and W. G. N. Slinn, pp. 181–188, Elsevier Sci., New York, 1983.

Brasseur, G., J. J. Orlando, and G. S. Tyndall, *Atmospheric Chemistry and Global Change*, Oxford Univ. Press, New York, 1999.

Chatfield, R. B., and P. J. Crutzen, Sulfur dioxide in remote oceanic air: Cloud transport of reactive precursors, *J. Geophys. Res.*, *89*, 7111–7132, 1984.

Chen, J.-P., and D. Lamb, The role of precipitation microphysics in the selective filtration of air entering the upper troposphere, in *Conference on Cloud Physics*, pp. 479–484, Am. Meteorol. Soc., Boston, Mass., 1990.

Chen, J.-P., and D. Lamb, Simulation of cloud microphysics and chemical processes using a multicomponent framework, I, Description of the microphysical model, *J. Atmos. Sci.*, *51*, 2613–2630, 1994.

Cho, H.-R., M. Niewiadomski, J. V. Iribarne, and O. Melo, A model of the effect of cumulus clouds on the redistribution and transformation of pollutants, *J. Geophys. Res.*, *94*, 12,895–12,910, 1989.

Clapsaddle, C., and D. Lamb, Sorption behavior of SO_2 on ice at temperatures between -30°C and -5°C, *Geophys. Res. Lett.*, *16*, 1173–1176, 1989.

Cohan, D. S., M. G. Schultz, D. J. Jacob, B. G. Heikes, and D. R. Blake, Convective injection and photochemical decay of peroxides in the tropical upper troposphere: Methyl iodide as a tracer of marine convection, *J. Geophys. Res.*, *104*, 5717–5724, 1999.

Crutzen, P. J., and M. G. Lawrence, The impact of precipitation scavenging on the transport of trace gases: A 3-dimensional model sensitivity study, *J. Atmos. Chem.*, *37*, 81–112, 2000.

Dickerson, R. R., et al., Thunderstorms: An important mechanism in the transport of air pollutants, *Science*, *235*, 460–465, 1987.

Diehl, K., S. K. Mitra, and H. R. Pruppacher, A laboratory study of the uptake of hno$_3$ and hcl vapor by snow crystals and ice spheres at temperatures between 0 and -40 degrees C, *Atmos. Environ.*, *29*, 975–981, 1995.

Dye, J. E., et al., An overview of the Stratospheric-Tropospheric Experiment: Radiation, Aerosols, and Ozone (STERAO)-Deep Convection experiment with results for the July 10, 1996 storm, *J. Geophys. Res.*, *105*, 10,023–10,045, 2000.

Easter, R. C., and J. M. Hales, Interpretations of the OSCAR data for reactive gas scavenging, in *Precipitation Scavenging, Dry Deposition, and Resuspension*, edited by H. R. Pruppacher, R. G. Semonin, and W. G. N. Slinn, pp. 649–662, Elsevier Sci., New York, 1983.

Flossmann, A. I., and W. Wobrock, Venting of gases by convective clouds, *J. Geophys. Res.*, *101*, 18,639–18,649, 1996.

Giorgi, F., and W. L. Chameides, Rainout lifetimes of highly soluble aerosols and gases as inferred from simulations with a general circulation model, *J. Geophys. Res.*, *91*, 14,367–14,376, 1986.

Hauf, T., P. Schulte, R. Alheit, and H. Schlager, Rapid vertical trace gas transport by an isolated midlatitude thunderstorm, *J. Geophys. Res.*, *100*, 22,957–22,970, 1995.

Hobbs, P. V., *Ice Physics*, Clarendon, Oxford, England, 1974.

Iribarne, J. V., and T. Pyshnov, The effect of freezing on the composition of supercooled droplets, I, Retention of HCl, HNO_3, NH_3, and H_2O_2, *Atmos. Environ., Part A*, *24A*, 383–387, 1990.

Jaeglé, L., et al., Observed OH and HO_2 in the upper troposphere suggest a major source from convective injection of peroxides, *Geophys. Res. Lett.*, *24*, 3181–3184, 1997.

Kreidenweis, S. M., Y. Zhang, and G. R. Taylor, The effects of clouds on aerosol and chemical species production and distribution, 2, Chemistry model description and sensitivity analysis, *J. Geophys. Res.*, *102*, 23,867–23,882, 1997.

Lamb, D., and R. Blumenstein, Measurement of the entrapment of sulfur dioxide by rime ice, *Atmos. Environ.*, *21*, 1765–1772, 1987.

Lelieveld, J., and P. J. Crutzen, The role of clouds in tropospheric photochemistry, *J. Atmos. Chem.*, *12*, 229–267, 1991.

Lin, Y.-L., R. D. Farley, and H. D. Orville, Bulk parameterization of the snow field in a cloud model, *J. Clim. Appl. Meteorol.*, *22*, 1065–1092, 1983.

Mari, C., D. J. Jacob, and P. Bechtold, Transport and scavenging of soluble gases in a deep convective cloud, *J. Geophys. Res.*, *105*, 22,255–22,267, 2000.

Mitchell, D. L., and D. Lamb, Influence of riming on the chemical composition of snow in winter orographic storms, *J. Geophys. Res.*, *94*, 14,830–14,840, 1989.

Pickering, K. E., J. R. Scala, A. M. Thompson, W.-K. Tao, and J. Simpson, A regional estimate of convective transport of CO from biomass burning, *Geophys. Res. Lett.*, *19*, 289–292, 1992a.

Pickering, K. E., A. M. Thompson, J. R. Scala, W.-K. Tao, R. R. Dickerson, and J. Simpson, Free tropospheric ozone production following entrainment of urban plumes into deep convection, *J. Geophys. Res.*, *97*, 17,985–18,000, 1992b.

Prather, M. J., and D. J. Jacob, A persistent imbalance in HO_x and NO_x photochemistry of the upper troposphere driven by deep tropical convection, *Geophys. Res. Lett.*, *24*, 3189–3192, 1997.

Pruppacher, H. R., and J. D. Klett, *Microphysics of Clouds and Precipitation*, Kluwer Acad., Norwell, Mass., 1997.

Rutledge, S. A., D. A. Hegg, and P. V. Hobbs, A numerical model for sulfur and nitrogen scavenging in narrow cold-frontal rainbands, 1, Model description and discussion of microphysical fields, *J. Geophys. Res.*, *91*, 14,385–14,402, 1986.

Scala, J. R., K. E. Pickering, W.-K. Tao, J. Simpson, and R. R. Dickerson, Convective transport and mixing of tracers by midlatitude squall-type mesoscale convective systems, in *Conference on Atmospheric Chemistry*, pp. 61–66, Am. Meteorol. Soc., Boston, Mass., 1993.

Scala, J. R., et al., Cloud draft structure and trace gas transport, *J. Geophys. Res.*, *95*, 17,015–17,030, 1990.

Schwartz, S. E., Mass-transport considerations pertinent to aqueous phase reactions of gases in liquid-water clouds, in *Chemistry of Multiphase Atmospheric Systems*, edited by W. Jaeschke, pp. 415–471, Springer-Verlag, New York, 1986.

Skamarock, W. C., et al., Numerical simulations of the July 10 Stratospheric-Tropospheric Experiment: Radiation, Aerosols, and Ozone/Deep Convection Experiment convective system: Kinematics and transport, *J. Geophys. Res.*, *105*, 19,973–19,990, 2000.

Snider, J. R., and J. Huang, Factors influencing the retention of hydrogen peroxide and molecular oxygen in rime ice, *J. Geophys. Res.*, *103*, 1405–1415, 1998.

Snider, J. R., D. C. Montague, and G. Vali, Hydrogen peroxide retention in rime ice, *J. Geophys. Res.*, *97*, 7569–7578, 1992.

Tabazadeh, A., and R. P. Turco, A model for heterogeneous chemical processes on the surfaces of ice and nitric acid trihydrate particles, *J. Geophys. Res.*, *98*, 12,727–12,740, 1993.

Tao, W.-K., and J. Simpson, Goddard cumulus ensemble model, I, Model description, *TAO*, *4*, 35–72, 1993.

Thompson, A. M., K. E. Pickering, R. R. Dickerson, W. G. Ellis, Jr., D. J. Jacob, J. R. Scala, W.-K. Tao, D. P. McNamara, and J. Simpson, Convective transport over the central United States and its role in regional CO and ozone budgets, *J. Geophys. Res.*, *99*, 18,703–18,711, 1994.

Tremblay, A., Cumulus cloud transport, scavenging, and chemistry: Observations and simulations, *Atmos. Environ.*, *21*, 2345–2364, 1987.

Wang, C., and J. S. Chang, A three-dimensional numerical model of cloud dynamics, microphysics, and chemistry, 1, Concepts and formulation, *J. Geophys. Res.*, *98*, 14,827–14,844, 1993a.

Wang, C., and J. S. Chang, A three-dimensional numerical model of cloud dynamics, microphysics, and chemistry, 4, Cloud chemistry and precipitation chemistry, *J. Geophys. Res.*, *98*, 16,799–16,808, 1993b.

Wang, C., and P. J. Crutzen, Impact of a simulated severe local storm on the redistribution of sulfur dioxide, *J. Geophys. Res.*, *100*, 11,357–11,367, 1995.

Wicker, L. J., and W. C. Skamarock, A time splitting scheme for the elastic equations incorporating second-order Runge-Kutta time differencing, *Mon. Weather Rev.*, *126*, 1992–1999, 1998.

Wicker, L. J., and R. B. Wilhelmson, Simulation and analysis of tornado development and decay within a three-dimensional supercell thunderstorm, *J. Atmos. Sci.*, *52*, 2675–2703, 1995.

M. C. Barth and W. C. Skamarock, National Center for Atmospheric Research, P.O. Box 3000, Boulder, CO 80307. (barthm@ucar.edu)

A. L. Stuart, Department of Civil and Environmental Engineering, Stanford University, Stanford, CA 94305.

(Received October 25, 2000; revised February 21, 2001; accepted February 28, 2001.)